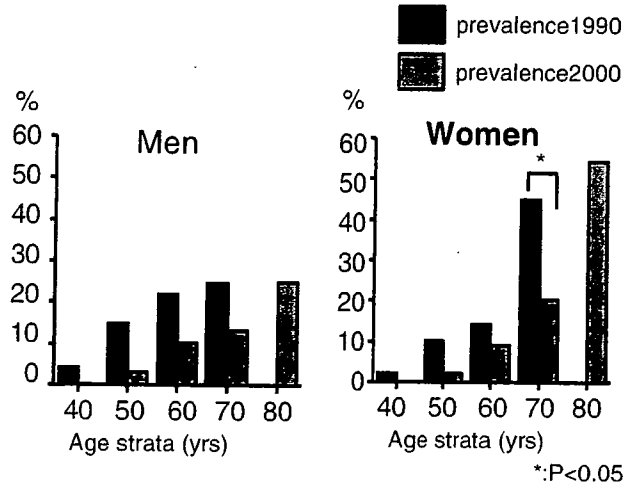

Fig. 2 Comparison of prevalence for vertebral fractures in the same age groups among participants in the X-ray examinations performed in 1990 and 2000

initial X-ray survey are shown in Table 2. The cumulative incidence of VFx including subjects with previous VFx after 10 years increased with age in both men and women.

After excluding cases with previous VFx, the cumulative incidence of first VFx for participants in their 40s, 50s, 60s, and 70s increased with age in both men and women, and was higher in women than in men in all age strata, except the 40s.

Although no association was identified between the cumulative incidence among participants with previous VFx and age in both men and women, cumulative incidence was significantly higher for subjects with previous VFx than for subjects without previous VFx in both men and women ($P<0.05$).

4. Cumulative incidence of VFx among survivors

The cumulative incidences of VFx among cases with first VFx for survivors in their 40s, 50s, 60s, and 70s were 2.9%, 2.8%, 8.6%, and 21.1% for men, and 2.1%, 7.0%, 18.9%, and 31.3% for women, respectively. The cumulative incidence of the first VFx among survivors increased with age in both men and women, and was higher in women than in men in all age strata, except in the 40s.

The cumulative incidences of VFx including subjects who had suffered from previous fractures or with increased numbers of VFx after 10 years for survivors in their 40s, 50s, 60s, and 70s were 2.9%, 10.3%, 13.2%, and 30.0% for men, and 2.1%, 6.8%, 23.1%, and 45.8% for women, respectively, suggesting an increase with age. Cumulative incidence was, again, significantly higher for subjects with previous VFx than for those without previous VFx in both men and women ($P<0.01$).

Discussion

The present study evaluated the prevalence and cumulative incidence of VFx over 10 years using radiographic diagnosis after the performance of two radiographic examinations of the thoracolumbar spine in anteroposterior and lateral views of population-based subjects.

Compared with hip fractures, epidemiological studies of VFx have been less available. One reason for this is the fact that VFx are not always symptomatic, and longitudinal

Table 2 Cumulative incidences over 10 years for men and women classified by the presence or absence of VFx at the initial survey

		All participants			With presence of VFx at the initial survey			With absence of VFx at the initial survey		
Birth cohort	Age strata at the initial survey (yrs)	No. of new VFx 1990–2000	No. of participants initial X-ray survey 1990	Cumulative incidence (%)	No. of new VFx cases 1990–2000	No. of participants initial survey 1990	Cumulative incidence (%)	No. of new VFx cases 1990–2000	No. of participants initial survey 1990	Cumulative incidence (%)
Men	Total	16	194	8.2	7	32	21.9	9	162	5.6
1940–49	40–49	1	47	2.1	0	2	0.0	1	45	2.2
1930–39	50–59	4	48	8.3	2	7	28.6	2	41	4.9
1920–29	60–69	5	50	10.0	3	11	27.3	2	39	5.1
1910–19	70–79	6	49	12.2	2	12	16.7	4	37	10.8
Women	Total	24	196	12.2	9	35	25.7	16	161	9.9
1940–49	40–49	1	48	2.1	0	1	0.0	1	47	2.1
1930–39	50–59	3	49	6.1	1	5	20.0	2	44	4.5
1920–29	60–69	9	50	18.0	3	7	42.9	6	43	14.0
1910–19	70–79	11	49	22.4	5	22	22.7	6	27	22.2

population surveys are required to clarify epidemiological indices. The present study used subjects representative of the whole town, and careful follow-up was performed. One limitation was the use of a relatively small number of fractures and small study population to determine the prevalence and cumulative incidence of VFx. However, few such longitudinal observational studies with high participation rates have been reported, representing the principal strength of this study.

Another reason for the scarcity of data on this subject is the lack consensus regarding the definition of VFx [25]. The present study utilized the diagnostic criteria of the Japan Bone and Mineral Society, as these criteria are the most popular and most commonly used in various clinical fields in Japan. These criteria seem to use the kind of semiquantative (SQ) method advocated by Genant et al. [26]. From the perspective of grading in SQ methods, the criteria of the Japan Bone and Mineral Society correspond to grades above SD2. The epidemiological indices in the present study, thus, did not include cases classifiable as SD1, suggesting that the results obtained using Japanese criteria might represent an underestimation compared to other results diagnosed using SQ methods.

Population-based prevalence studies of VFx have been performed in Western countries, such as the USA [27], Denmark [28, 29], Finland [30], Sweden [31, 32], the Netherlands [33], England [34, 35], and France [36, 37], and in a multicenter study involving 19 European countries [38]. In Asia, the prevalence of VFx has been reported in Taiwan [39], China [40], and Japan [18, 19, 24]. Cummings et al. compared the results of population-based studies of radiological VFx prevalence in women ≥50-years-old between Europe, Minnesota (USA), Hawaii (USA), Hiroshima (Japan), Taiwan, and Beijing (China) [41]. In this comparison, the prevalence of VFx among women >70-years-old was higher in Japan than in the USA or China, and was as high as that in Europe. The prevalence of VFx in the mountainous area of the present study was much higher than that in Hiroshima, an urban area, suggesting that regional differences in VFx might be present in Japan.

The present study clarified differences in the prevalence of VFx for given age strata between birth cohorts. The comparison of data collected in 1990 and 2000 showed improvements over time for men and women in their 50s, 60s, and 70s. A previous report has already noted that BMD data from 1990 and 2000 showed significant improvements for men in their 60s and for women in their 50s [23], concluding that this might predict a decrease in the prevalence of osteoporosis in the near future in Japan. The present results suggest that the prevalence of not only osteoporosis, but also osteoporotic fractures, could decrease in the future in Japan. Fujiwara et al. assessed the effects of birth cohort on the incidence of VFx in Hiroshima, and reported that incidence decreased by a factor of 0.5 in men and 0.6 in women with each succeeding birth decade [17]. The present data are consistent with these findings.

This low prevalence of VFx in more recent birth cohorts may reflect nutritional improvements, in addition to BMD improvements. As noted elsewhere [23], nationwide nutritional surveys have reported the mean calcium intake as 253 mg/day in 1946 (1st survey), 338 mg/day in 1955, 465 mg/day in 1965, and 552 mg/day in 1975 [42], representing a dramatic increase. These nutritional improvements might be expected to increase body build and BMD, and, thus, decrease the prevalence of VFx in all age groups. Another possible reason for the decreasing prevalence of VFx might be the effects of action taken for the prevention of osteoporosis by the government and academic societies. To achieve the prevention of osteoporosis, the Ministry of Health, Labour and Welfare recommended all that communities start BMD screening for middle-aged and elderly female residents in 1995. These examinations in various communities have enabled many women to become more aware of osteoporosis. Moreover, the Japan Osteoporosis Foundation and the Japan Osteoporosis Society, which were established in 1991 and 1999, respectively, have been conducting public education campaigns to inform the general population about osteoporosis and risk factors. These efforts by both the government and academic societies might have resulted in the decreasing prevalence of VFx.

Regarding the incidence of VFx, while some epidemiological studies have been reported from Western countries [43–45], the only investigation from Japan was reported by Fujiwara et al. [18]. Fujiwara et al. performed radiographic examinations in 1994–1995, with follow-up at an average of 4 years, and clarified the incidence of VFx in their Hiroshima cohort. Incidences of VFx in this Hiroshima cohort increased with age, particularly after about 60 years of age, and women displayed a nearly two-fold greater incidence of VFx than men. The incidence of VFx was much higher in individuals with previous VFx than in those without previous VFx. As cumulative incidence was clarified in the present study, rather than incidence, direct comparison of the present results with those of Fujiwara et al. might be incorrect. However, findings in the present study, such as age-dependency, sex differences, and higher incidence in individuals with previous VFx than in those without previous VFx, are consistent with the results of the previous investigation in Hiroshima.

The cumulative incidence for participants at the initial survey in the present study could be considered as a 10-year probability according to age. In this mountain village, 12.2% of men and 22.4% of women in their 70s will suffer new morphometric VFx in the next 10 years. Kanis et al. reported the 10-year probability of clinical VFx in female

participants in the European Prospective Osteoporosis Study [46]. The 10-year probability of clinical VFx among women with a 0 Z-score of amplitude-dependent speed of sound on quantitative ultrasound (QUS) measurements was 3.9% at 70 years old, 4.5% at 75 years old, and 4.9% at 80 years old. Although only about one-third of morphometric fractures reportedly come to medical attention [43], the present results indicated much higher incidences than those described by Kanis et al. Although the future incidence of VFx in the Japanese population could be predicted to decrease, elderly individuals seem to remain at high risk. To reduce the incidence and prevalence of osteoporosis and osteoporotic fractures, further epidemiological research is needed to facilitate the development of affordable strategies for the early identification of high-risk individuals.

Acknowledgments This work was supported by Grants-in-Aid for Scientific Research C16590512 from the Ministry of Education, Science, Sports, and Culture in Japan, H16-Chihou Kossetsu-021, H17-Meneki-009 from the Ministry of Health, Labour and Welfare, and the grant from the Japan Osteoporosis Society.

References

1. Burger H, Van Daele PL, Grashuis K, Hofman A, Grobbee DE, Schutte HE, Birkenhanger JC, Pols HA (1977) Vertebral deformities and functional impairment in men and women. J Bone Miner Res 12(1):152–157
2. Ross PD (1977) Clinical consequences of vertebral fractures. Am J Med 103(2A):30S–43S
3. Nevitt MC, Ettinger B, Black DM, Stone K, Jamal SA, Ensrud K, Segal M, Genant HK, Cummings RS (1988) The association of radiographically detected vertebral fractures with back pain and function: a prospective study. Ann Intern Med 128(10):793–800
4. Yamaguchi T, Sugimoto T, Yamada H, Kanzawa M, Yano S, Yamauchi M, Chihara K (2002) The presence and severity of vertebral fractures is associated with the presence of esophageal hiatal hernia in postmenopausal women. Osteoporos Int 13(4):331–336
5. Gold DT, Lyles KW, Shipp KM, Drezner MK (2001) Osteoporosis and its nonskeletal consequences: their impact on treatment decisions. In: Marcus R, Feldman D, Kelsey J (eds) Osteoporosis, 2nd edn. Academic Press, San Diego, California, pp 819–829
6. Leech JA, Dulberg C, Kellie S, Pattee L, Gay J (1990) Relationship of lung function to severity of osteoporosis in women. Am Rev Respir Dis 141(1):68–71
7. Gold DT (1966) The clinical impact of vertebral fractures: quality of life in women with osteoporosis. Bone 18(3 Suppl):185S–189S
8. Oleksik A, Lips P, Dawson A, Minshall ME, Shen W, Cooper C, Kanis J (2000) Health-related quality of life in postmenopausal women with low BMD with or without prevalent vertebral fractures. J Bone Miner Res 15(7):1384–1392
9. Ross PD, Davis JW, Epstein RS, Wasnich RD (1991) Pre-existing fractures and bone mass predict vertebral fracture incidence in women. Ann Intern Med 114(11):919–923
10. Ross PD, Genant HK, Davis JW, Miller PD, Wasnich RD (1993) Predicting vertebral fracture incidence from prevalent fractures and bone density among non-black, osteoporotic women. Osteoporos Int 3(3):120–126
11. Nevitt MC, Ross PD, Palermo L, Musliner T, Genant HK, Thompson DE (1999) Association of prevalent vertebral fractures, bone density, and alendronate treatment with incident vertebral fractures: effect of number and spinal location of fractures. The Fracture Intervention Trial Research Group. Bone 25(5):613–619
12. Black DM, Arden NK, Palermo L, Pearson J, Cummings SR (1999) Prevalent vertebral deformities predict hip fractures and new vertebral deformities but not wrist fractures. Study of Osteoporotic Fractures Research Group. J Bone Miner Res 14 (5):821–828
13. Burger H, van Daele PLA, Algra D, Hofman A, Grobbee DE, Schutte HE, Birkenhager JC, Pols HA (1994) Vertebral deformities as predictors of non-vertebral fractures. BMJ 309:991–992
14. Center JR, Nguyen TV, Schneider D, Sambrook PN, Eisman JA (1999) Mortality after all major types of osteoporotic fracture in men and women: an observational study. Lancet 353(9156):878–882
15. Ensrud KE, Thompson DE, Cauly JA, Nevitt MC, Kado DM, Hochberg MC, Santora AC 2nd, Black DM (2000) Prevalent vertebral deformities predict mortality and hospitalization in older women with low bone mass. Fracture Intervention Trial Research Group. J Am Geriatr Soc 48(3):241–249
16. Johnell O, Kanis JA, Oden A, Sernbo I, Redlund-Johnell I, Petterson C, De Laet C, Jonsson B (2004) Mortality after osteoporotic fractures. Osteoporos Int 15(1):38–42
17. Fujiwara S, Mizuno S, Ochi Y, Sasaki H, Kodama K, Russell WJ, Hosoda Y (1991) The incidence of thoracic vertebral fractures in a Japanese population, Hiroshima and Nagasaki, 1958–1986. J Clin Epidemiol 44(10):1007–1014
18. Fujiwara S, Kasagi F, Masunari N, Naito K, Suzuki G, Fukunaga M (2003) Fracture prediction from bone mineral density in Japanese men and women. J Bone Miner Res 18(8):1547–1553
19. Kitazawa A, Kushida K, Yamazaki K, Inoue T (2001) Prevalence of vertebral fractures in a population-based sample in Japan. J Bone Miner Metab 19(2):115–118
20. Kasamatsu T, Morioka S, Hashimoto T, Kinoshita H, Yamada H, Tamaki T (1991) Epidemiological study on the bone mineral density of inhabitants in Miyama Village, Wakayama prefecture (Part I). Background of study population and sampling method. J Bone Miner Metab 9(Suppl 1):50–55
21. Kinoshita H, Danjoh S, Yamada H, Tamaki T, Kasamatsu T, Ueda A, Hashimoto T (1991) Epidemiological study on the bone mineral density of inhabitants in Miyama Village, Wakayama prefecture (part II). Bone mineral density of the spine and proximal femur. J Bone Miner Metab 9(Suppl 1):56–60
22. Yoshimura N, Kinoshita H, Danjoh S, Takijiri T, Morioka S, Kasamatsu T, Sakata K, Hashimoto T (2002) Bone loss at the lumbar spine and the proximal femur in a rural Japanese community, 1990–2000: the Miyama study. Osteoporos Int 13 (10):803–808
23. Yoshimura N, Kinoshita H, Danjoh S, Yamada H, Tamaki T, Morioka S, Kasamatsu T, Hashimoto T, Inoue T (1995) Prevalence of vertebral fractures in a rural Japanese population. J Epidemiol 5:171–175
24. Inoue T (1990) Clinical features and findings, osteoporosis (in Japanese). Bone 4:39–47
25. National Osteoporosis Foundation Working Group on Vertebral Fractures (1995) Report assessing vertebral fractures. J Bone Miner Res 10:518–523
26. Genant HK, Wu CY, Van Kujuk C, Nivitt MC (1993) Vertebral fracture assessment using a semiquantative technique. J Bone Miner Res 8:1137–1148
27. Ross PD, Fujiwara S, Huang C, Davis JW, Epstein RS, Wasnich RD, Kodama K, Melton LJ 3rd (1995) Vertebral fracture prevalence in women in Hiroshima compared to Caucasians or Japanese in the US. Int J Epidemiol 24(6):1171–1177

28. Hansen MA, Overgaard, Nielsen VAH, Jensen GF, Gotfredsen A, Christiansen C (1992) No secular increase in the prevalence of vertebral fractures due to postmenopausal osteoporosis. Osteoporos Int 2(5):241–246
29. Jensen GF, Christiansen C, Boesen J, Hegedus V, Transbol I (1982) Epidemiology of postmenopausal spinal and long bone fractures: a unifying approach to postmenopausal osteoporosis. Clin Orthop 166:75–81
30. Harna M, Heliovaara M, Aromaa A, Knekt P (1986) Thoracic spine compression fractures in Finland. Clin Orthop 205:188–194
31. Bengner UU, Johnell O, Redlund-Johnell I (1988) Changes in incidence and prevalence of vertebral fractures during 30 years. Calcif Tissue Int 42(5):293–296
32. Hasserius R, Redlund-Johnell I, Mellstrom D, Johansson C, Nilsson BE, Johnell O (2001) Vertebral deformation in urban Swedish men and women: prevalence based on 797 subjects. Acta Orthop Scand 72(3):273–278
33. Pluijm SMF, Tromp AM, Smit JH, Deeg DJH, Lips P (2000) Consequences of vertebral deformities in older men and women. J Bone Miner Res 15(8):1564–1572
34. Cooper C, Shah S, Hand DJ, Adams J, Compston J, Davie M, Woolf A (1991) Screening for vertebral osteoporosis using individual risk factors. The Multicentre Vertebral Fracture Study Group. Osteoporos Int 2(1):48–53
35. Spector TD, McCloskey EV, Dogle DV, Kanis JA (1993) Prevalence of vertebral fracture in women and the relationship with bone density and symptoms: the Chingford Study. J Bone Miner Res 8(7):817–822
36. Szulc P, Marchand F, Felsenberg D, Delmas PD (1998) Prevalence of vertebral deformities according to the diagnostic method. Rev Rhum Engl Ed 65(4):245–256
37. Grados F, Marcelli C, Dargent-Molina P, Roux C, Vergnol JF, Meunier PJ, Fardellone P (2004) Prevalence of vertebral fractures in French women older than 75 years from the EPIDOS study. Bone 34(2):362–367
38. O'Neill TW, Felsenberg D, Varlow J, Cooper C, Kanis JA, Silman AJ (1996) The prevalence of vertebral deformity in European men and women: the European Vertebral Osteoporosis Study. J Bone Miner Res 11(7):1010–1018
39. Tsai K, Twu S, Chieng P, Yang R, Lee T (1996) Prevalence of vertebral fractures in Chinese men and women in urban Taiwanese communities. Calcif Tissue Int 59(4):249–253
40. Ling X, Cummings SR, Mingwei Q, Xihe Z, Xioashu C, Nevitt M, Stone K (2000) Vertebral fractures in Beijing, China: the Beijing Osteoporosis Project. J Bone Miner Res 15 (10):2019–2025
41. Cummings SR, Melton KJ 3rd (2002) Epidemiology and outcomes of osteoporotic fractures. Lancet 359(9319):1761–1767
42. Office for Lifestyle-Related Diseases Control, Health Services Bureau, Ministry of Health, Labour and Welfare (1998) The trend of dietary circumstances after World War II. Annual report of the national nutrition survey, Japan (in Japanese). Daiichi Shuppan, Tokyo, Japan, pp 145–150
43. Cooper C, Aekinson EJ, O'Fallon WM, Melton LJ 3rd (1992) Incidence of clinically diagnosed vertebral fractures: a population-based study in Rochester, Minnesota, 1985–1989. J Bone Miner Res 7(2):449–456
44. Sanders KM, Pasco JA, Ugoni AM, Nicholson GC, Seeman E, Martin TJ, Skoric B, Panahi S, Kotowicz MA (1998) The exclusion of high trauma fractures may underestimate the prevalence of bone fragility fractures in the community: the Geelong Osteoporosis Study. J Bone Miner Res 13(8):1337–1342
45. The European Prospective Osteoporosis Study Group (2002) Incidence of vertebral fracture in Europe: results from the European Prospective Osteoporosis Study (EPOS). J Bone Miner Res 17(4):716–724
46. Kanis JA, Johnell O, Oden A, De Laet C, De Terlizzi F (2005) Ten-year probabilities of clinical vertebral fractures according to phalangeal quantitative ultrasonography. Osteoporos Int 16 (9):1065–1070

ARTHRITIS & RHEUMATISM
Vol. 54, No. 8, August 2006, pp 2462–2470
DOI 10.1002/art.22041

Contribution of Runt-Related Transcription Factor 2 to the Pathogenesis of Osteoarthritis in Mice After Induction of Knee Joint Instability

Satoru Kamekura,[1] Yosuke Kawasaki,[1] Kazuto Hoshi,[1] Takashi Shimoaka,[1] Hirotaka Chikuda,[1] Zenjiro Maruyama,[1] Toshihisa Komori,[2] Shingo Sato,[3] Shu Takeda,[3] Gerard Karsenty,[4] Kozo Nakamura,[1] Ung-il Chung,[1] and Hiroshi Kawaguchi[1]

Objective. **By producing instability in mouse knee joints, we attempted to determine the involvement of runt-related transcription factor 2 (RUNX-2), which is required for chondrocyte hypertrophy, in the development of osteoarthritis (OA).**

Methods. **An experimental mouse OA model was created by surgical transection of the medial collateral ligament and resection of the medial meniscus of the knee joints of heterozygous RUNX-2–deficient ($Runx2^{+/-}$) mice and wild-type littermates. Cartilage destruction and osteophyte formation in the medial tibial cartilage were compared by histologic and radiographic analyses. Localization of type X collagen and matrix metalloproteinase 13 (MMP-13) was examined by immunohistochemistry. Localization of RUNX-2 was determined by X-Gal staining in heterozygous RUNX-2–deficient mice with the *lacZ* gene insertion at the *Runx2*-deletion site ($Runx2^{+/lacZ}$). Messenger RNA levels of type X collagen, MMP-13, and RUNX-2 were examined by real-time reverse transcriptase–polymerase chain reaction analysis.**

Results. **RUNX-2 was induced in the articular cartilage of wild-type mice at the early stage of OA, almost simultaneously with type X collagen but earlier than MMP-13. $Runx2^{+/-}$ and $Runx2^{+/lacZ}$ mice showed normal skeletal development and articular cartilage; however, after induction of knee joint instability, they exhibited decreased cartilage destruction and osteophyte formation, along with reduced type X collagen and MMP-13 expression, as compared with wild-type mice.**

Conclusion. **RUNX-2 contributes to the pathogenesis of OA through chondrocyte hypertrophy and matrix breakdown after the induction of joint instability.**

Osteoarthritis (OA), a chronic degenerative joint disorder characterized by articular cartilage destruction and osteophyte formation, is a major cause of disability in the elderly. Despite significant demand for more information, risk factors for this disease, as identified by epidemiologic studies, have to date been limited to age, obesity, trauma history, occupation, and sex (1,2). Since these factors are closely related to the accumulation of mechanical loading on joints, mechanical instability of the joints may play some role in OA pathogenesis. In an effort to clarify the mechanisms whereby joint instability leads to the development of OA, experimental animal models of OA induced by producing instability in the joints by surgical intervention have been developed in dogs, rabbits, guinea pigs, and rats (3–9). Due to recent progress in mouse genomics and the availability of transgenic and knockout mice, the mouse is currently the ideal animal for molecular study. Using a microsurgical technique to produce instability in the knee joints of mice, we established models of mechanical instability–induced OA that were reproducible and resembled OA in humans (10).

Supported by a Grant-in-Aid for Scientific Research from the Japanese Ministry of Education, Culture, Sports, Science, and Technology (15209049).

[1]Satoru Kamekura, MD, Yosuke Kawasaki, MD, Kazuto Hoshi, MD, Takashi Shimoaka, MD, Hirotaka Chikuda, MD, Zenjiro Maruyama, MD, Kozo Nakamura, MD, Ung-il Chung, MD, Hiroshi Kawaguchi, MD, PhD: Faculty of Medicine, University of Tokyo, Tokyo, Japan; [2]Toshihisa Komori, MD: Nagasaki University Graduate School of Biomedical Sciences, Nagasaki, Japan; [3]Shingo Sato, MD, Shu Takeda, MD: Tokyo Medical and Dental University, Tokyo, Japan; [4]Gerard Karsenty, MD: Baylor College of Medicine, Houston, Texas.

Address correspondence and reprint requests to Hiroshi Kawaguchi, MD, PhD, Sensory and Motor System Medicine, Faculty of Medicine, University of Tokyo, Hongo 7-3-1, Bunkyo, Tokyo 113-8655, Japan. E-mail: kawaguchi-ort@h.u-tokyo.ac.jp.

Submitted for publication November 24, 2005; accepted in revised form May 16, 2006.

We and other investigators (10–12) have previously reported that the early stage of OA is characterized by hypertrophic differentiation of chondrocytes, as determined by type X collagen expression in the superficial and middle zones of cartilage above the tidemark. Runt-related transcription factor 2 (RUNX-2), which was originally isolated on the basis of its ability to activate transcription of the osteoblast-specific osteocalcin gene (13,14), is known to be the only transcription factor that is required for chondrocyte hypertrophy (15–20). In the present study, therefore, we examined RUNX-2 expression in knee cartilage during OA progression, using our experimental mouse model. In addition, we investigated the functional involvement of RUNX-2 by comparing OA progression in heterozygous RUNX-2–deficient mice with that in wild-type mice.

MATERIALS AND METHODS

Animals. All experiments were performed according to the protocol approved by the Animal Care and Use Committee of the University of Tokyo. For the expression levels of type X collagen, matrix metalloproteinase 13 (MMP-13), type II collagen (CII), and RUNX-2 during OA progression, we used conventional wild-type C57BL/6 mice (8 weeks old) obtained from Charles River Japan (Yokohama, Japan). For the functional analyses of RUNX-2, we used heterozygous RUNX-2–deficient mice ($Runx2^{+/-}$) (129SVJ and C57BL/6 mixed background) that were created as previously reported (21), since homozygous RUNX-2–deficient ($Runx2^{-/-}$) mice died just after birth. $Runx2^{+/-}$ mice and the control wild-type littermates were generated by mating $Runx2^{+/-}$ mice. For the detection of RUNX-2 expression in situ, heterozygous RUNX-2–deficient mice with the *lacZ* gene inserted at the site of the *Runx2* gene deletion in 1 allele ($Runx2^{+/lacZ}$) (CBA and C57BL/6 mixed background) (22) were used (kindly provided by Dr. M. J. Owen, GlaxoSmithKline, London, UK). In total, we used 42 conventional mice, 42 $Runx2^{+/-}$ mice, 42 wild-type mice, and 24 $Runx2^{+/lacZ}$ mice.

OA model. The surgical procedure to create an experimental OA model was performed on 8-week-old mice as previously described (10). Briefly, under general anesthesia using pentobarbiturate (0.5 mg/10 gm body weight, intraperitoneally) (Sigma, St. Louis, MO), the bilateral hind limbs were prepared for aseptic surgery. The knee joint was exposed following a medial capsular incision and gentle lateral displacement of the extensor muscle, without transection of the patellar ligament. Then, the medial collateral ligament was transected, and the medial meniscus was removed using a surgical microscope and microsurgical technique. After replacement of the extensor muscle, the medial capsular incision was sutured, and the skin was closed. During the procedure, close attention was paid not to injure the articular cartilage. A sham operation was performed on the contralateral knee joint using the same approach, with no ligament transection or menisectomy. The animals were then allowed unrestricted activity, food, and water ad libitum.

Histologic analysis. At the indicated time points after surgery, the mice were killed, and the entire knee joints were dissected and fixed for 4 hours at 4°C in 4% paraformaldehyde buffered with phosphate buffered saline (PBS; pH 7.4). The specimens were decalcified for 2 weeks with 10% EDTA (pH 7.4) at 4°C. After the specimens were dehydrated with an increasing concentration of ethanol and embedded in paraffin, 4 μm of the frontal section was cut from the joints. Sections were stained with Safranin O–fast green. Development of OA was quantified by our original histologic grading scale of 0–4 for cartilage destruction (0 = no apparent changes, 1 = loss of superficial zone in articular catilage, 2 = defects limited to above tidemark, 3 = defects extending to calcified cartilage, and 4 = exposure of subchondral bone to cartilage destruction) and 0–3 for osteophyte formation (0 = none, 1 = formation of cartilage-like tissue [cartilaginous outgrowth], 2 = increase in cartilaginous matrix, and 3 = endochondral ossification or osteophyte formation), as previously described (10). The grades were scored as the most severe changes among >20 serial sections. A single observer (KH) who was blinded to the experimental group scored the sections.

Histomorphometric measurements of trabecular bone volume (bone volume/tissue volume) in the subchondral region of medial tibial joints were made according to the guidelines of the American Society of Bone and Mineral Research (23). Measurements of 2 separate sections per knee joint, spaced 50 μm apart, were obtained with an image analyzer (Histometry RT camera; System Supply, Nagano, Japan).

Immunohistochemistry. Immunohistochemical localization of type X collagen, MMP-13, and CII were performed in deparaffinized sections, as previously described (24). The sections were treated with 0.3% H_2O_2 in PBS for 30 minutes and with 2.5% hyaluronidase (Sigma) for 30 minutes. After blocking with 1% bovine serum albumin (Sigma) in PBS for 1 hour at room temperature, sections were incubated with polyclonal rabbit antibodies against rat type X collagen and CII (LSL, Tokyo, Japan), and polyclonal goat antibodies against rabbit MMP-13 (Chemicon, Temecula, CA) at a dilution of 1:100 for 24 hours at 4°C. As negative controls, we used nonimmune rabbit or goat IgG of the same dilution instead of the primary antibodies. The sections were rinsed in PBS and incubated for 20 minutes with Alexa Fluor 488–conjugated goat antibodies against rabbit IgG for type X collagen and with horseradish peroxidase–conjugated goat antibodies against rabbit IgG (ICN Biomedicals, Aurora, OH) for MMP-13 and CII. Visualization of immunoreactivity was performed using Alexa Fluor 488 fluorescence for type X collagen and by diaminobenzidine staining with methyl green counterstaining for MMP-13 and CII.

X-Gal staining. Since neither antibodies nor riboprobes worked appropriately in the localization of RUNX-2 by immunostaining or in situ hybridization of the cartilage tissue of adult mice, respectively, we used X-Gal staining to examine LacZ expression under control of RUNX-2 promoter activation in $Runx2^{+/lacZ}$ mice. Eight-week-old male $Runx2^{+/lacZ}$ mice that underwent the microsurgery described above were killed at 2, 4, and 8 weeks, and the entire knee joint was dissected. The specimens were fixed in 2% paraformaldehyde buffered with PBS (pH 7.4) for 1 hour at 4°C. To detect β-galactosidase activity, the tissues were stained with X-Gal, as previously described (22). The specimens were decalcified for

2 weeks with 10% EDTA (pH 7.4) at 4°C. After dehydration with an increasing concentration of ethanol and embedding in paraffin, 4 μm of the frontal section was cut from the joints.

Real-time reverse transcriptase–polymerase chain reaction (RT-PCR) analysis. To determine the messenger RNA (mRNA) levels of RUNX-2, type X collagen, and MMP-13 in OA cartilage, we collected the medial tibial cartilage from OA and sham-operated knee joints 2, 4, and 8 weeks after surgery, as previously described (25). Total RNA was extracted from the samples using the chaotropic TRIzol method, followed by isogen–chloroform extraction and isopropanol precipitation (Nippon Gene, Tokyo, Japan), according to the manufacturer's instructions. Total mRNA (1 μg) was reverse transcribed using Superscript reverse transcriptase with random hexamer (Takara Shuzo, Shiga, Japan), and 1 μl of each reverse transcriptase reaction was used as a template for the second-step SYBR Green real-time RT-PCR. The full-length or partial-length complementary DNA of target genes, including PCR amplicon sequences, was amplified by PCR, cloned into pCR-TOPO Zero II or pCR-TOPO II vectors (Invitrogen, Carlsbad, CA), and used as standard templates after linearization. QuantiTect SYBR Green PCR Master Mix (Qiagen, Chatsworth, CA) was used for the second-step SYBR Green real-time RT-PCR according to the manufacturer's instructions. SYBR Green PCR amplification and real-time fluorescence detection were performed using an ABI Prism 7700 sequence detection system (Applied Biosystems, Foster City, CA). All reactions were run in quadruplicate. Copy numbers of target gene mRNA in each total RNA were calculated by reference to standard curves and were adjusted to the mouse standard total RNA (ABI) with the mouse actin as an internal control. PCR amplification was performed using the following gene-specific primer pairs: for type X collagen, sense 5′-CATAAAGGGCCCACTTGCTA-3′ and antisense 5′-TGGCTGATATTCCTGGTGGT-3′; for MMP-13, sense 5′-AGGCCTTCAGAAAAGCCTTC-3′ and antisense 5′-TCCTTGGAGTGATCCAGACC-3′; for RUNX-2, sense 5′-CCCAGCCACCTTTACCTACA-3′ and antisense 5′-TATGGAGTGCTGCTGGTCTG-3′; and for actin, sense 5′-AGATGTGGATCAGCAAGCAG-3′ and antisense 5′-GCGCAAGTTAGGTTTTGTCA-3′. Data were normalized by the average mRNA level before the operation (time 0), and expressed as the mean ± SEM in 8–10 mice per group per time point.

Radiographic analysis. Radiographs of the knee joints of wild-type and Runx2$^{+/-}$ mice were obtained 12 weeks after surgery under general anesthesia using a soft x-ray apparatus (CMB-2; Softex, Tokyo, Japan).

Statistical analysis. Group means were compared by analysis of variance, and significance of differences was determined by post hoc testing with Bonferroni adjustment. P values less than 0.05 were considered significant.

RESULTS

Time course of type X collagen, MMP-13, and CII expression in OA cartilage. Among the 4 types of experimental mouse OA models, we used the medial model in this study, with transection of the medial collateral ligament and resection of the medial meniscus of the knee of 8-week-old male mice (10). This model exhibits the disorder in the medial portion, resembling the area most affected by OA in humans, and is suitable for observation of the early stage of OA, since it displays a relatively slow progression of the condition. In fact, Safranin O staining showed matrix degradation at 4 weeks after surgery and cartilage destruction into the middle zone at 8 weeks (Figure 1A).

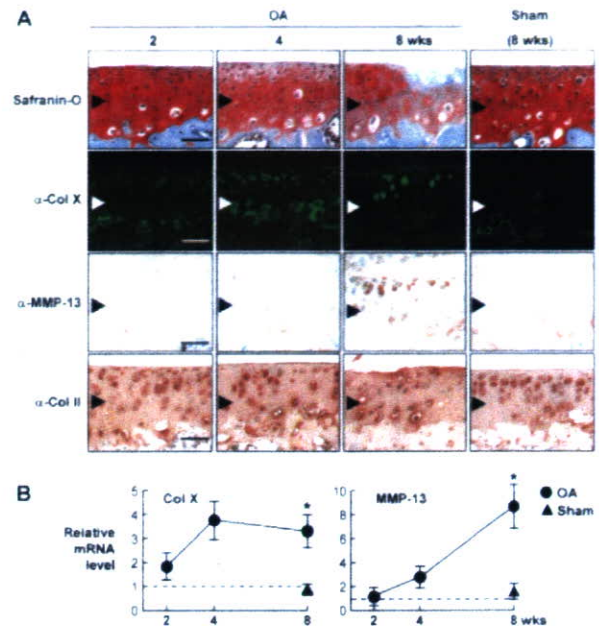

Figure 1. Time course of expression of type X collagen (Col X), matrix metalloproteinase 13 (MMP-13), and type II collagen (CII) in the medial portion of tibial cartilage during the development of osteoarthritis (OA) by induction of joint instability. Eight-week-old male wild-type mice underwent medial collateral ligament transection and medial meniscus resection in the right knee joint, as described in Materials and Methods. A sham operation was performed on the left knee joint, using the same approach. **A,** Representative histologic features of frontal sections of the right knee 2, 4, and 8 weeks after surgery and of the left knee 8 weeks after surgery. Safranin O staining and immunohistochemical staining with type X collagen, MMP-13, and CII antibodies were performed. Immunoreactivity was visualized with Alexa Fluor 488 fluorescence for type X collagen, and with diaminobenzidine staining with methyl green counterstaining for MMP-13 and CII. **Arrowheads** indicate the levels of the tidemark. Bars = 100 μm. **B,** Type X collagen and MMP-13 mRNA levels in medial tibial cartilage extracts from OA and sham-operated knee joints, determined by real-time reverse transcriptase–polymerase chain reaction analysis. Data were normalized to the average mRNA level before the operation (time 0) (set at 1) and are expressed as the mean ± SEM of 8 samples per group per time. * = $P < 0.01$ versus sham-operated knees.

Immunohistochemical analyses were performed

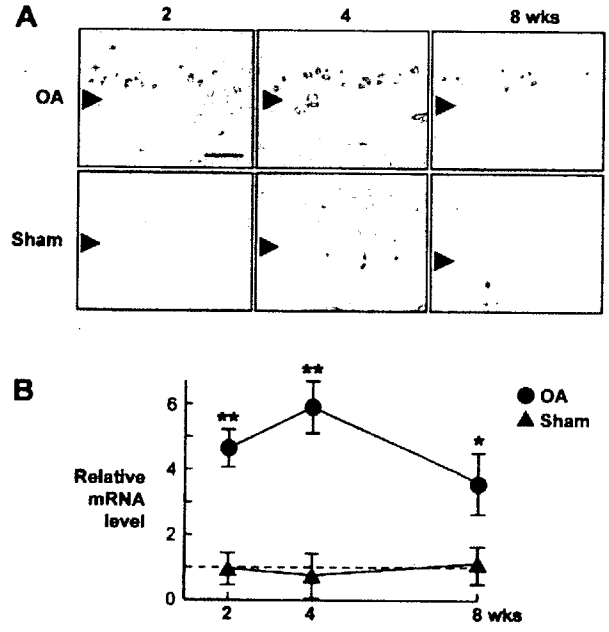

Figure 2. Time course of runt-related transcription factor 2 (RUNX-2) expression in the medial portion of tibial cartilage during development of osteoarthritis (OA) by induction of joint instability. **A,** Representative histologic features of frontal sections 2, 4, and 8 weeks after surgery. For runt-related transcription factor 2 (RUNX-2) expression in situ, 8-week-old male Runx2$^{+/lacZ}$ mice (n = 4 per group per time) underwent microsurgery or sham operation as described in Materials and Methods, and the specimens were stained with X-Gal to detect β-galactosidase activity. **Arrowheads** indicate the level of the tidemark. Bar = 100 μm. **B,** RUNX-2 mRNA level in medial tibial cartilage extracts from OA and sham-operated knee joints of conventional wild-type mice, as determined by real-time reverse transcriptase–polymerase chain reaction analysis. Data were normalized to the average mRNA level before the operation (time 0) (set at 1) and are expressed as the mean ± SEM of 8 samples per group per time. * = $P < 0.05$; ** = $P < 0.01$ versus sham-operated knees.

in this model to assess the time course of type X collagen and MMP-13 expression, which in our previous study (10), were shown to be most strongly induced among collagens and MMPs during OA progression. Although type X collagen expression was limited to the deep calcified zone below the tidemark in the sham-operated knee and at 2 weeks after OA induction, at 4 weeks, it appeared in the superficial and middle zones above the tidemark. MMP-13 expression was not detected above the tidemark at 2 or 4 weeks; however, it was clearly localized in hypertrophic chondrocytes at 8 weeks. The up-regulation of type X collagen and MMP-13 occurred only in the medial portion of the knee joint, where the mechanical instability was loaded, but not in the unaffected lateral portion (data not shown). In contrast, the immunolocalization of CII was unaltered during OA progression, as we previously reported (10). Quantification of mRNA levels in cartilage extracts by real-time RT-PCR analysis confirmed the distinct time course of the expression of type X collagen and MMP-13 (Figure 1B). These findings suggest that articular chondrocytes undergo hypertrophic differentiation in response to joint instability at an early stage, and the hypertrophic chondrocytes express MMP-13, which may degrade the cartilage matrix.

Time course of RUNX-2 expression in OA cartilage. We examined the involvement of RUNX-2, a transcriptional activator that has been known to induce both chondrocyte hypertrophy and MMP-13 expression (15–20,26,27). We initially created the medial OA model in the knee joint of Runx2$^{+/lacZ}$ mice, and examined RUNX-2 expression by X-Gal staining. Time course analysis of the sham-operated cartilage revealed that RUNX-2 expression was positive in some chondrocytes in calcified cartilage below the tidemark, but was not visible in cells above the tidemark (Figure 2A). In contrast, RUNX-2 expression was induced above the tidemark in the OA cartilage as early as 2 weeks, was enhanced at 4 weeks, and decreased thereafter until 8 weeks. This RUNX-2 induction also occurred only in the medial portion of the joint, where the mechanical instability was loaded, but not in the unaffected lateral portion (data not shown). Real-time RT-PCR analysis of cartilage extracts from conventional wild-type mice confirmed the time course of the RUNX-2 mRNA level during OA progression (Figure 2B), suggesting the involvement of RUNX-2 in the early stage of OA.

Effects of RUNX-2 insufficiency on type X collagen and MMP-13 expression in OA cartilage. To determine the involvement of RUNX-2 in the induction of type X collagen and MMP-13 during OA progression, we examined the expression in Runx2$^{+/-}$ mice. The Runx2$^{+/-}$ mice, as well as Runx2$^{+/lacZ}$ mice, showed normal skeletal development and articular cartilage under physiologic conditions (data not shown). We therefore created the medial OA model in 8-week-old mice and compared the expression of type X collagen and MMP-13 in the medial tibial cartilage during OA progression. We first confirmed, by real-time RT-PCR analysis, that RUNX-2 mRNA levels were increased at 4 and 8 weeks after surgery in wild-type mice, while levels at both times were significantly reduced to less than half in Runx2$^{+/-}$ mice (Figure 3B). Immunohistochemical analysis showed that type X collagen expression was visible above the tidemark in the articular cartilage of wild-type mice at 4 and 8 weeks after surgery; however,

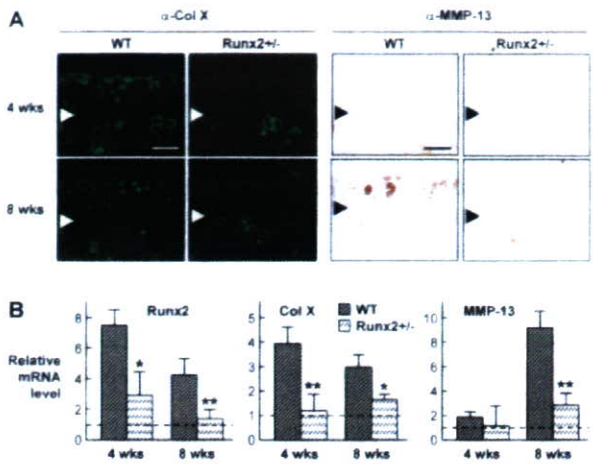

Figure 3. Type X collagen, MMP-13, and RUNX-2 expression in the medial portion of tibial cartilage of wild-type (WT) and $Runx2^{+/-}$ mice during development of OA by induction of joint instability. Eight-week-old male wild-type and $Runx2^{+/-}$ mice underwent microsurgery to induce OA in the knee joints. Samples were prepared and stained as described in Figure 1. **A,** Representative immunohistochemical staining of frontal sections 4 and 8 weeks after surgery. **Arrowheads** indicate the level of the tidemark. Bars = 100 μm. **B,** RUNX-2, type X collagen, and MMP-13 mRNA levels in medial tibial cartilage extracts from wild-type and $Runx2^{+/-}$ mice, determined by real-time reverse transcriptase–polymerase chain reaction analysis. Data were normalized to the average mRNA level before the operation (time 0) (set at 1) and are expressed as the mean and SEM of 8 samples per group per time. * = $P < 0.05$; ** = $P < 0.01$ versus wild-type mice. See Figure 1 for other definitions.

this was rarely seen in the articular cartilage of $Runx2^{+/-}$ mice, except in the calcified cartilage below the tidemark (Figure 3A). MMP-13 expression was also increased above the tidemark in the articular cartilage of wild-type mice at 8 weeks, which was significantly reduced in the cartilage of $Runx2^{+/-}$ mice. Real-time RT-PCR analysis confirmed that both type X collagen and MMP-13 mRNA levels were decreased by RUNX-2 insufficiency (Figure 3B), indicating that chondrocyte hypertrophy and MMP-13 induction during OA progression are at least partly mediated by RUNX-2.

Effect of RUNX-2 insufficiency on OA progression. To further investigate the contribution of RUNX-2 to the development of OA, we next compared the susceptibility of cartilage destruction and osteophyte formation between joints from wild-type and $Runx2^{+/-}$ mice, using joint instability in the medial model. Safranin O staining of cartilage in wild-type mice showed that cartilage destruction progressed into the middle zone by 8 weeks after surgery and reached the calcified cartilage layer across the tidemark by 12 weeks (Figure 4A). The cartilage destruction in $Runx2^{+/-}$ mice was much milder, however, and it was confined within the middle zone throughout the observation period. The $Runx2^{+/lacZ}$ joint was confirmed to exhibit cartilage destruction similar to that of $Runx2^{+/-}$ mice and milder than wild-type mice. Quantification by our original grading system (10) revealed significant reduction of cartilage destruction by the RUNX-2 insufficiency at 8 weeks and thereafter (Figure 4B).

Osteophyte formation, the other characteristic feature of OA, was detected at the medial edge of the joints of wild-type mice 12 weeks after surgery in both radiographic (Figure 5A) and histologic (Figure 5B) analyses. Joints in the $Runx2^{+/-}$ and $Runx2^{+/lacZ}$ mice showed decreased cartilaginous outgrowth and osteo-

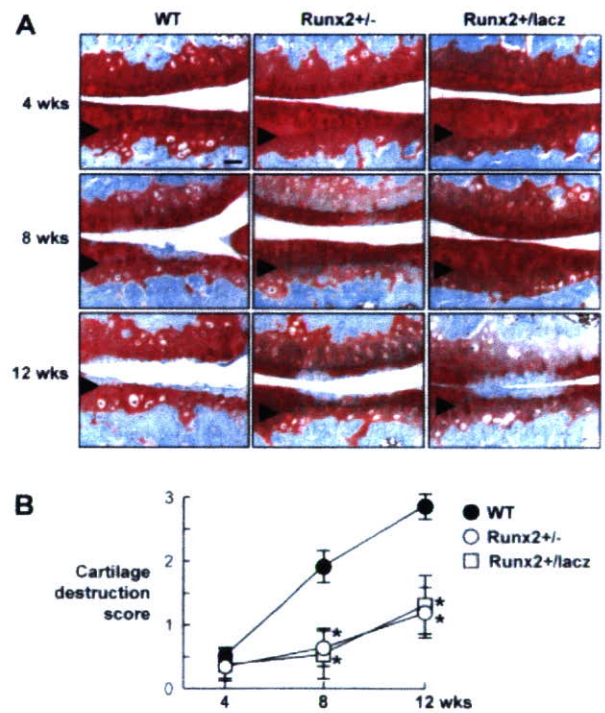

Figure 4. Time course of cartilage destruction in the medial portion of tibial cartilage of wild-type (WT), $Runx2^{+/-}$, and $Runx2^{+/lacZ}$ mice after induction of joint instability. Eight-week-old male mice underwent microsurgery to induce osteoarthritis in the knee joints, and the samples were prepared and stained. **A,** Representative histologic features (Safranin O staining) of frontal sections 4, 8, and 12 weeks after surgery. **Arrowheads** indicate the level of the tidemark. Bar = 100 μm. **B,** Histologic scoring of cartilage destruction according to the grading system described in Materials and Methods. Data are expressed as the mean ± SEM of 10 samples per genotype per time for wild-type and $Runx2^{+/-}$ mice, and of 4 samples per time for $Runx2^{+/LacZ}$ mice. * = $P < 0.01$ versus wild-type mice.

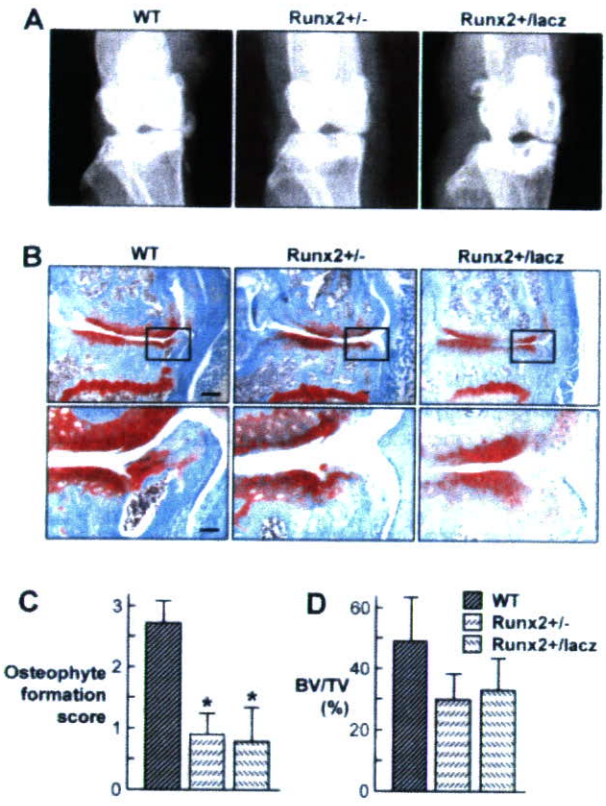

Figure 5. Osteophyte formation in the medial portion of tibial cartilage of wild-type (WT), Runx2$^{+/-}$, and Runx2$^{+/lacZ}$ mice 12 weeks after induction of joint instability. **A,** Representative anteroposterior radiographs. **B,** Representative histologic features of frontal sections (Safranin O staining). Boxed areas in the top row indicate the regions shown at higher magnification in the bottom row. Bars = 200 μm (top) and 50 μm (bottom). **C,** Histologic scoring of osteophyte formation according to the grading system described in Materials and Methods. **D,** Histomorphometric measurements of trabecular bone volume (bone volume/tissue volume [BV/TV]) in the subchondral region of medial tibial joints. Data in **C** and **D** are expressed as the mean and SEM of 10 samples per genotype per time for wild-type and Runx2$^{+/-}$ mice, and of 4 samples per time for Runx2$^{+/LacZ}$ mice. $* = P < 0.01$ versus wild-type mice.

phyte formation. Quantification by the osteophyte formation score (10) at 12 weeks confirmed the reduction by RUNX-2 insufficiency (Figure 5C). The trabecular bone volume in the subchondral region tended to be lower in mice with RUNX-2 insufficiency, although not statistically significant (Figure 5D). These findings demonstrate that RUNX-2 contributes to at least 2 characteristic features of OA: cartilage destruction and osteophyte formation under the unstable joint.

DISCUSSION

Although several studies have examined the expression of matrix proteins in OA cartilage using experimental models in larger animals, such as dogs and rabbits (3–7,9), the results have been inconsistent. For example, in rabbit models 1 study showed no alteration of CII expression (7), while another showed its up-regulation at region-specific sites (5). In canine models, CII expression was higher in OA knee joints, and expression progressed in one study (4) and decreased in another one (6). Other matrix proteins, such as aggrecan and fibromodulin, seem to be altered only at isolated time points (5,7).

Our previous immunohistochemical analyses using an experimental mouse OA model (medial model) showed no substantial change in CII, type IX collagen, MMP-2, MMP-3, or MMP-9 expression, but up-regulation of type X collagen and MMP-13 (10). The present time course analyses using the same model confirmed up-regulation of type X collagen and MMP-13 with no alteration of CII, by immunohistochemical and real-time RT-PCR analyses. In this model, definite increases in RUNX-2, type X collagen, and MMP-13 were seen at 2, 4, and 8 weeks, respectively, after surgery (Figures 1 and 2), while cartilage destruction became visible at 8 weeks (10). In addition, RUNX-2 insufficiency caused a decrease in cartilage destruction, along with a reduction in type X collagen and MMP-13 expression. Furthermore, transgenic mice expressing constitutively active MMP-13 are reported to exhibit articular cartilage destruction resembling OA (28). These findings indicate that induction of these molecules is the cause, not the effect, of the cartilage destruction.

Under physiologic conditions, articular cartilage does not show chondrocyte hypertrophy, but maintains the stable phenotype as a permanent cartilage. However, in OA articular cartilage, pathologic expression of type X collagen and other differentiation markers, including annexin VI, alkaline phosphatase, osteopontin, and osteocalcin, have been reported (11,12,29–31), indicating that OA articular cartilage cannot maintain the characteristics of the permanent cartilage, but gains those of the growth plate cartilage, which undergoes endochondral ossification. MMP-13, which potently degrades cartilage matrix with a preference for CII, is known to be induced in OA articular cartilage (32) and to be functionally involved in OA pathogenesis (28). This proteinase has been suggested to be induced in response to proinflammatory cytokines such as tumor necrosis factor

α (TNFα), interleukin-1 (IL-1), and IL-6 in articular cartilage under pathologic conditions, such as OA and rheumatoid arthritis (RA) (2,33). However, it is suspicious that these cytokines play significant roles in the development of OA. Our previous study showed that levels of TNFα, IL-1, IL-6, as well as fibroblast growth factor 2, in the synovial fluid from knee joints of patients with OA were much lower than those from patients with RA (34).

Furthermore, a recent study using a mouse OA model similar to ours (35) showed that mice lacking IL-1, IL-1β–converting enzyme, stromelysin 1, or inducible nitric oxide synthase unexpectedly exhibited an acceleration of cartilage destruction, implying that these proinflammatory factors do not stimulate, but rather inhibit, cartilage destruction. Instead, we propose that chondrocyte hypertrophy is important for MMP-13 induction in cartilage. There are well-ordered expression patterns of type X collagen and MMP-13 in the growth plate cartilage; only the highly differentiated cells in the type X collagen–positive hypertrophic chondrocytes are able to express MMP-13 (10,36,37). This sequence of expression may be essential for endochondral ossification that needs prior degradation of the cartilage matrix. The present time-course study also showed that MMP-13 expression occurred later than hypertrophic differentiation of OA chondrocytes, suggesting the principal role of chondrocyte hypertrophy in the development of OA.

Although several signaling molecules, including Indian hedgehog and parathyroid hormone–related peptide, have been shown in mouse genetics studies to regulate chondrocyte hypertrophy, RUNX-2 is known to be the only transcription factor that is necessary for hypertrophy, based on several lines of evidence. Runx2$^{-/-}$ mice show no hypertrophic chondrocytes in some skeletal elements (15,16), and expression of a dominant-negative *Runx2* mutation inhibits chondrocyte hypertrophy and ossification in vivo (18). Constitutive expression of RUNX-2 in prehypertrophic chondrocytes leads to premature and ectopic chondrocyte hypertrophy (17–19). In addition, endogenous RUNX-2 is known to be expressed mainly in prehypertrophic chondrocytes during endochondral ossification in skeletal development and growth (15,19). The present analysis also showed that RUNX-2 expression reached a maximum at 2–4 weeks and decreased at 8 weeks, suggesting that RUNX-2 is expressed in prehypertrophic chondrocytes that undergo hypertrophic differentiation and apoptosis thereafter in the OA cartilage as well.

The fact that type X collagen was induced shortly after RUNX-2 during OA progression is consistent with a recent finding that type X collagen is a direct transcriptional target of RUNX-2 by transactivation of the promoter (20). However, the time lag between RUNX-2 and MMP-13 expression was inconsistent with previous reports showing the direct activation of MMP-13 transcription by RUNX-2 (26,27). RUNX-2 may therefore induce type X collagen expression directly, and then the hypertrophic chondrocytes express MMP-13 during the development of OA.

The mechanism whereby mechanical instability induces RUNX-2 expression in articular cartilage remains unclarified. RUNX-2 was recently reported to be a target of mechanical signals, mainly in osteoblasts, causing anabolic action in bone. Low-level stretching, as well as extracellular nucleotides released in response to mechanical stimuli, up-regulates not only RUNX-2 expression, but also its DNA binding activity in cultured osteoblasts (38,39). This effect in bone was shown to be modulated by activation of ERK MAPK and protein kinase C.

In contrast, more complicated mechanoresponsive mechanisms appear to evolve in chondrocytes. Although tensile strain increased RUNX-2 expression, hydrostatic pressure decreased it somewhat in cultured primary chondrocytes (40). In fact, our preliminary experiment using the culture of chondrocytes isolated from the growth plate of wild-type and Runx2$^{+/-}$ mice, as described previously (41), failed to show induction of RUNX-2 by stretching stimulation using the Flexercell culture system (data not shown). Since we also could not find RUNX-2 induction in OA superficial chondrocytes earlier than 2 weeks after surgery (data not shown), it is likely that the induction is not directly from mechanical instability, but occurs by way of changes in other molecules. Establishment of a chondrocyte culture system that accurately reproduces the in vivo environment of OA articular cartilage induced by joint instability will be essential to elucidate the molecular network mediating RUNX-2 expression.

Accumulation of mechanical loading and the subsequent cartilage destruction were confined to the medial portion of the tibial cartilage in the present model, and the changes in RUNX-2, type X collagen, and MMP-13 were detected mainly in the affected medial portion. However, a previous study (9) has shown that expression levels of CII, type I collagen, and YKL-40 were up-regulated independently of joint localization during the early stages in an experimental canine OA model (3). Another study of expression levels of CII, aggrecan, biglycan, decorin, fibromodulin, and MMPs 1,

3, and 13 demonstrated significant region-specific changes in a rabbit OA model (5). Although the present study failed to detect the up-regulation of RUNX-2, type X collagen, or MMP-13 in the unaffected lateral portion, further studies of region-specific expression of a subset of transcription factors, cytokines, matrix molecules, proteinases, and proteinase inhibitors should elucidate the molecular network underlying the OA pathogenesis in the whole joint.

Although OA has long been considered to be primarily a cartilage disorder associated with focal articular cartilage degradation, recent studies suggest the involvement of subchondral trabecular bone in the pathophysiology (8,42,43). The increased subchondral bone stiffness is suggested to reduce the ability to dissipate the load and distribute the strain generated within the joint, which augments peak dynamic forces in the overlying articular cartilage and can accelerate its damage over time. In fact, the present study showed a decrease in the subchondral trabecular bone volume in mice with RUNX-2 insufficiency, although it was not statistically significant. Considering that *Runx2* is originally known as a master gene for bone formation, we cannot deny the possibility that reduced cartilage destruction due to RUNX-2 insufficiency is at least partly secondary to the decreased subchondral bone. Further analyses using bone- and cartilage-specific RUNX-2–deficient mice driven by type I collagen and CII promoters, respectively, would determine the tissue-specific role of RUNX-2 during OA progression.

We herein propose a mechanism of OA development, in which RUNX-2 expression induced by mechanical instability causes pathologic hypertrophic differentiation of articular chondrocytes, which then produces MMP-13 that degrades cartilage matrix. We certainly do not think that MMP-13 is the sole proteinase for cartilage degradation in OA. In fact, deletion of active ADAMTS-5 (aggrecanase 2), another member of the metalloproteinase family, was recently reported to prevent cartilage destruction in mouse arthritis models (44,45). We speculate that the cartilage degradation by these metalloproteinases may lead to osteophyte formation through endochondral ossification at the edge of the articular cartilage to which new blood vessels are accessible by adjacent synovial or fibrous tissue. But it may result in cartilage destruction without ossification at the avascular central area.

The fact that RUNX-2 insufficiency prevented both cartilage destruction and osteophyte formation without affecting physiologic skeletal conditions suggests that this molecule can clinically be a therapeutic target of these disorders, since RUNX-2 is known to be induced in human OA cartilage (46). Mutations in the *Runx2* gene cause cleidocranial dysplasia not only in mice, but also in humans (22,47,48). Although various types of the human *RUNX-2* gene, including chromosomal translocations, deletions, insertions, nonsense, missense, and splice-site mutations, have been reported to cause a wide spectrum of phenotypic variability, ranging from primary dental anomalies to all typical features plus osteoporosis, future studies on the susceptibility of OA in these patients will provide invaluable information on the possibility that RUNX-2 is a clinical target for this common joint disorder.

ACKNOWLEDGMENTS

We thank Dr. Michael Owen for providing the $Runx2^{+/lacZ}$ mice. We also thank Reiko Yamaguchi, Mizue Ikeuchi, Shinpei Sotoyama, and Motoki Miyazawa for their excellent technical assistance.

REFERENCES

1. Doherty M. Risk factors for progression of knee osteoarthritis. Lancet 2001;358:775–6.
2. Poole AR, Howell DS. Etiopathies of osteoarthritis. In: Moskowitz RW, Howell DS, Altman RD, Buckwalter JA, Goldberg VM, editors. Osteoarthritis: Diagnosis and medical/surgical management. 3rd ed. Philadelphia: Saunders; 2001. p. 29–47.
3. Pond MJ, Nuki G. Experimentally-induced osteoarthritis in the dog. Ann Rheum Dis 1973;32:387–8.
4. Matyas JR, Ehlers PF, Huang D, Adams ME. The early molecular natural history of experimental osteoarthritis. I. Progressive discoordinate expression of aggrecan and type II procollagen messenger RNA in the articular cartilage of adult animals. Arthritis Rheum 1999;42:993–1002.
5. Le Graverand MP, Eggerer J, Vignon E, Otterness IG, Barclay L, Hart DA. Assessment of specific mRNA levels in cartilage regions in a lapine model of osteoarthritis. J Orthop Res 2002;20:535–44.
6. Matyas JR, Huang D, Chung M, Adams ME. Regional quantification of cartilage type II collagen and aggrecan messenger RNA in joints with early experimental osteoarthritis. Arthritis Rheum 2002;46:1536–43.
7. Bluteau G, Gouttenoire J, Conrozier T, Mathieu P, Vignon E, Richard M, et al. Differential gene expression analysis in a rabbit model of osteoarthritis induced by anterior cruciate ligament (ACL) section. Biorheology 2002;39:247–58.
8. Hayami T, Pickarski M, Wesolowski GA, McLane J, Bone A, Destefano J, et al. The role of subchondral bone remodeling in osteoarthritis: reduction of cartilage degeneration and prevention of osteophyte formation by alendronate in the rat anterior cruciate ligament transection model. Arthritis Rheum 2004;50:1193–206.
9. Lorenz H, Wenz W, Ivancic M, Steck E, Richter W. Early and stable upregulation of collagen type II, collagen type I and YKL40 expression levels in cartilage during early experimental osteoarthritis occurs independent of joint location and histological grading. Arthritis Res Ther 2005;7:R156–65.
10. Kamekura S, Hoshi K, Shimoaka T, Chung U, Chikuda H, Yamada T, et al. Osteoarthritis development in novel experimental mouse models induced by knee joint instability. Osteoarthritis Cartilage 2005;13:632–41.

11. Von der Mark K, Kirsch T, Nerlich A, Kuss A, Weseloh G, Gluckert K, et al. Type X collagen synthesis in human osteoarthritic cartilage: indication of chondrocyte hypertrophy. Arthritis Rheum 1992;35:806–11.
12. Boos N, Nerlich AG, Wiest I, von der Mark K, Ganz R, Aebi M. Immunohistochemical analysis of type-X-collagen expression in osteoarthritis of the hip joint. J Orthop Res 1999;17:495–502.
13. Ducy P, Zhang R, Geoffroy V, Ridall AL, Karsenty G. Osf2/Cbfa1: a transcriptional activator of osteoblast differentiation. Cell 1997;89:747–54.
14. Karsenty G, Wagner EF. Reaching a genetic and molecular understanding of skeletal development [review]. Dev Cell 2002;2:389–406.
15. Inada M, Yasui T, Nomura S, Miyake S, Deguchi K, Himeno M, et al. Maturational disturbance of chondrocytes in Cbfa1-deficient mice. Dev Dyn 1999;214:279–90.
16. Kim IS, Otto F, Zabel B, Mundlos S. Regulation of chondrocyte differentiation by Cbfa1. Mech Dev 1999;80:159–70.
17. Enomoto H, Enomoto-Iwamoto M, Iwamoto M, Nomura S, Himeno M, Kitamura Y, et al. Cbfa1 is a positive regulatory factor in chondrocyte maturation. J Biol Chem 2000;275:8695–702.
18. Ueta C, Iwamoto M, Kanatani N, Yoshida C, Liu Y, Enomoto-Iwamoto M, et al. Skeletal malformations caused by overexpression of Cbfa1 or its dominant negative form in chondrocytes. J Cell Biol 2001;153:87–100.
19. Takeda S, Bonnamy JP, Owen MJ, Ducy P, Karsenty G. Continuous expression of Cbfa1 in nonhypertrophic chondrocytes uncovers its ability to induce hypertrophic chondrocyte differentiation and partially rescues Cbfa1-deficient mice. Genes Dev 2001;15:467–81.
20. Zheng Q, Zhou G, Morello R, Chen Y, Garcia-Rojas X, Lee B. Type X collagen gene regulation by Runx2 contributes directly to its hypertrophic chondrocyte-specific expression in vivo. J Cell Biol 2003;162:833–42.
21. Komori T, Yagi H, Nomura S, Yamaguchi A, Sasaki K, Deguchi K, et al. Targeted disruption of Cbfa1 results in a complete lack of bone formation owing to maturational arrest of osteoblasts. Cell 1997;89:755–64.
22. Otto F, Thornell AP, Crompton T, Denzel A, Gilmour KC, Rosewell IR, et al. Cbfa1, a candidate gene for cleidocranial dysplasia syndrome, is essential for osteoblast differentiation and bone development. Cell 1997;89:765–71.
23. Parfitt AM, Drezner MK, Glorieux FH, Kanis JA, Malluche H, Meunier PJ, et al. Bone histomorphometry: standardization of nomenclature, symbols, and units. J Bone Miner Res 1987;2:595–610.
24. Hoshi K, Komori T, Ozawa H. Morphological characterization of skeletal cells in Cbfa1-deficient mice. Bone 1999;25:639–51.
25. Xu L, Peng H, Wu D, Hu K, Goldring MB, Olsen BR, et al. Activation of the discoidin domain receptor 2 induces expression of matrix metalloproteinase 13 associated with osteoarthritis in mice. J Biol Chem 2005;280:548–55.
26. Jimenez MJ, Balbin M, Lopez JM, Alvarez J, Komori T, Lopez-Otin C. Collagenase 3 is a target of Cbfa1, a transcription factor of the runt gene family involved in bone formation. Mol Cell Biol 1999;19:4431–42.
27. Porte D, Tuckermann J, Becker M, Baumann B, Teurich S, Higgins T, et al. Both AP-1 and Cbfa1-like factors are required for the induction of interstitial collagenase by parathyroid hormone. Oncogene 1999;18:667–78.
28. Neuhold LA, Killar L, Zhao W, Sung ML, Warner L, Kulik J, et al. Postnatal expression in hyaline cartilage of constitutively active human collagenase-3 (MMP-13) induces osteoarthritis in mice. J Clin Invest 2001;107:35–44.
29. Pullig O, Weseloh G, Gauer S, Swoboda B. Osteopontin is expressed by adult human osteoarthritic chondrocytes: protein and mRNA analysis of normal and osteoarthritic cartilage. Matrix Biol 2000;19:245–55.
30. Pullig O, Weseloh G, Ronneberger D, Kakonen S, Swoboda B. Chondrocyte differentiation in human osteoarthritis: expression of osteocalcin in normal and osteoarthritic cartilage and bone. Calcif Tissue Int 2000;67:230–40.
31. Pfander D, Swoboda B, Kirsch T. Expression of early and late differentiation markers (proliferating cell nuclear antigen, syndecan-3, annexin VI, and alkaline phosphatase) by human osteoarthritic chondrocytes. Am J Pathol 2001;159:1777–83.
32. Billinghurst RC, Dahlberg L, Ionescu M, Reiner A, Bourne R, Rorabeck C, et al. Enhanced cleavage of type II collagen by collagenases in osteoarthritic articular cartilage. J Clin Invest 1997;99:1534–45.
33. Vincenti MP, Brinckerhoff CE. Transcriptional regulation of collagenase (MMP-1, MMP-13) genes in arthritis: integration of complex signaling pathways for the recruitment of gene-specific transcription factors [review]. Arthritis Res 2002;4:157–64.
34. Manabe N, Oda H, Nakamura K, Kuga Y, Uchida S, Kawaguchi H. Involvement of fibroblast growth factor-2 in joint destruction of rheumatoid arthritis patients. Rheumatology (Oxford) 1999;38:714–20.
35. Clements KM, Price JS, Chambers MG, Visco DM, Poole AR, Mason RM. Gene deletion of either interleukin-1β, interleukin-1β–converting enzyme, inducible nitric oxide synthase, or stromelysin 1 accelerates the development of knee osteoarthritis in mice after surgical transection of the medial collateral ligament and partial medial meniscectomy. Arthritis Rheum 2003;48:3452–63.
36. D'Angelo M, Yan Z, Nooreyazdan M, Pacifici M, Sarment DS, Billings PC, et al. MMP-13 is induced during chondrocyte hypertrophy. J Cell Biochem 2000;77:678–93.
37. Jimenez MJ, Balbin M, Alvarez J, Komori T, Bianco P, Holmbeck K, et al. A regulatory cascade involving retinoic acid, Cbfa1, and matrix metalloproteinases is coupled to the development of a process of perichondrial invasion and osteogenic differentiation during bone formation. J Cell Biol 2001;155:1333–44.
38. Ziros PG, Gil AP, Georgakopoulos T, Habeos I, Kletsas D, Basdra EK, et al. The bone-specific transcriptional regulator Cbfa1 is a target of mechanical signals in osteoblastic cells. J Biol Chem 2002;277:23934–41.
39. Costessi A, Pines A, D'Andrea P, Romanello M, Damante G, Cesaratto L, et al. Extracellular nucleotides activate Runx2 in the osteoblast-like HOBIT cell line: a possible molecular link between mechanical stress and osteoblasts' response. Bone 2005;36:418–32.
40. Wong M, Siegrist M, Goodwin K. Cyclic tensile strain and cyclic hydrostatic pressure differentially regulate expression of hypertrophic markers in primary chondrocytes. Bone 2003;33:685–93.
41. Shimoaka T, Kamekura S, Chikuda H, Hoshi K, Chung UI, Akune T, et al. Impairment of bone healing by insulin receptor substrate-1 deficiency. J Biol Chem 2004;279:15314–22.
42. Radin EL, Rose RM. Role of subchondral bone in the initiation and progression of cartilage damage. Clin Orthop Relat Res 1986;213:34–40.
43. Burr DB. The importance of subchondral bone in osteoarthrosis [review]. Curr Opin Rheumatol 1998;10:256–62.
44. Glasson SS, Askew R, Sheppard B, Carito B, Blanchet T, Ma HL, et al. Deletion of active ADAMTS5 prevents cartilage degradation in a murine model of osteoarthritis. Nature 2005;434:644–8.
45. Stanton H, Rogerson FM, East CJ, Golub SB, Lawlor KE, Meeker CT, et al. ADAMTS5 is the major aggrecanase in mouse cartilage in vivo and in vitro. Nature 2005;434:648–52.
46. Wang X, Manner PA, Horner A, Shum L, Tuan RS, Nuckolls GH. Regulation of MMP-13 expression by RUNX2 and FGF2 in osteoarthritic cartilage. Osteoarthritis Cartilage 2004;12:963–73.
47. Mundlos S, Otto F, Mundlos C, Mulliken JB, Aylsworth AS, Albright S, et al. Mutations involving the transcription factor CBFA1 cause cleidocranial dysplasia. Cell 1997;89:773–9.
48. Otto F, Kanegane H, Mundlos S. Mutations in the RUNX2 gene in patients with cleidocranial dysplasia [review]. Hum Mutat 2002;19:209–16.

ELSEVIER

Autonomic Neuroscience: Basic and Clinical 128 (2006) 96–100

AUTONOMIC NEUROSCIENCE: Basic & Clinical

www.elsevier.com/locate/autneu

Short communication

Extracorporeal shockwaves induce the expression of ATF3 and GAP-43 in rat dorsal root ganglion neurons

Ryo Murata [a,*], Seiji Ohtori [a], Nobuyasu Ochiai [a], Norimasa Takahashi [a], Takashi Saisu [b], Hideshige Moriya [a], Kazuhisa Takahashi [a], Yuichi Wada [c]

[a] *Department of Orthopaedic Surgery, Graduate School of Medicine, Chiba University, Chiba, Japan*
[b] *Division of Orthopaedic Surgery, Chiba Children's Hospital, Chiba, Japan*
[c] *Department of Orthopaedic Surgery, Teikyo University Ichihara Hospital, Ichihara, Chiba, Japan*

Received 22 October 2005; received in revised form 11 April 2006; accepted 13 April 2006

Abstract

Although extracorporeal shockwave has been applied in the treatment of various diseases, the biological basis for its analgesic effect remains unclear. Therefore, we investigated the dorsal root ganglion neurons of rats following shockwave exposure to the footpad to elucidate its effect on the peripheral nervous system. We used activating transcription factor 3 (ATF3) and growth-associated phosphoprotein (GAP-43) as markers for nerve injury and axonal regeneration, respectively. The average number of neurons immunoreactive for ATF3 increased significantly in the treated rats at all experimental time points, with 78.3% of those neurons also exhibiting immunoreactivity for GAP-43. Shockwave exposure induced injury of the sensory nerve fibers within the exposed area. This phenomenon may be linked to the desensitization of the exposure area, not the cause of pain, considering clinical research with a particular absence of painful adverse effect. Subsequent active axonal regeneration may account for the reinnervation of exposed area and the amelioration of the desensitization.

Keywords: Shockwave; Analgesic effect; Nerve fiber; Injury; Regeneration

Extracorporeal shockwave therapy (ESW) has become better known as an approach for the management of various painful orthopedic disorders (Gerdesmeyer et al., 2003; Rompe et al., 1996, 2004). Despite the increasing recognition of ESW, only a few studies have investigated its biological effects on the nervous system and the mechanism of its analgesic effect (Maier et al., 2003; Haake et al., 2002).

We have previously shown that ESW of the rat footpad caused degeneration and reinnervation of sensory nerve fibers innervating the skin (Ohtori et al., 2001). ESW also caused a decrease in immunoreactivity for calcitonin gene-related peptide (CGRP) in dorsal root ganglion (DRG) neurons (Takahashi et al., 2003). The biological effects of ESW in other components of the sensory nervous system such as the DRG and spinal cord warrant further investigation.

Activating transcription factor 3 (ATF3) is specifically induced in DRG neurons and the spinal cord neurons after nerve injury. ATF3 is a member of the ATF/CREB family of transcription factors and its expression is induced in a variety of tissues exposed to stress (Hai et al., 1999). Although its function has not been clearly elucidated, ATF3 is widely regarded as a specific neuronal marker of nerve injury (Hai et al., 1999; Tsujino et al., 2000). On the other hand, growth-associated phosphoprotein (GAP-43) has emerged as one of the most useful markers of axonal regeneration (Skene and Willard, 1981), and is expressed at particularly high levels in developing neurons and elongating axonal growth cones (Jacobson et al., 1986). Nerve injury leads to increased synthesis of GAP-43 in adult neurons (Coggins and Zwiers, 1991). If ESW to the skin were to have effects on DRG neurons, observed changes in expression of these markers

* Corresponding author. Tel./fax: +81 43 226 2117.
E-mail address: drryokun@yahoo.co.jp (R. Murata).

1566-0702/$ - see front matter © 2006 Elsevier B.V. All rights reserved.
doi:10.1016/j.autneu.2006.04.003

may provide insight into the biological effects of ESW on the peripheral nervous system. With this in mind, we investigated changes in ATF3 and GAP-43 expression profiles in DRG neurons following ESW of the rat footpad.

Experiments were conducted in accordance with the guidelines for animal experimentation of the Ethics Review Committee of Chiba University. Twenty-eight male Sprague–Dawley rats weighing 250–300 g were used. Rats receiving ESW (the ESW group) were generally anaesthetized with an intraperitoneal injection of 40 mg/kg sodium pentobarbital before shockwave exposure. Two-thousand shockwave pulses at an energy flux density of 0.08 mJ/mm^2 and a frequency of 4 Hz generated by a lithotripter (Dornier Med. Tech.; Epos®) were applied to the skin of footpads corresponding to the L4 and L5 dermatomes as previously described (Takahashi et al., 1994).

On 1, 2, 4, 7, 14 and 28 days after the shockwave exposure, four rats each in the ESW group were anesthetized with 40 mg/kg sodium pentobarbital and perfused transcardially with 0.9% saline, followed by 500 ml of 4% paraformaldehyde in a phosphate buffer (0.1 M, pH 7.4). After fixation, the L4 and L5 DRG of the rats were collected bilaterally. The other four rats received no shockwaves and were used as controls; the bilateral L4 and L5 DRG were collected in the same manner as for the ESW group. After storage in 0.01 M phosphate-buffered saline (PBS) containing 20% sucrose at 4 °C for 20 h, the specimens were serially sectioned on a cryostat at 20 μm intervals.

The sections were treated in blocking solution (0.01 M PBS containing 0.3% Triton X-100 and 1% normal goat serum) at room temperature for 90 min. They were then incubated at 4 °C for 20 h in rabbit antibody for ATF3 (1:200; Santa Cruz Biotechnology, Santa Cruz, CA) and mouse antibody for GAP-43 (1:1000; Sigma, St. Louis, MO) diluted in blocking solution. After they were washed three times in PBS, the sections were incubated with secondary antibodies (Alexa 594-labeled anti-mouse antibodies [1:250; Molecular Probes, Eugene, OR] and Alexa 488-labeled anti-rabbit antibodies [1:250; Molecular Probes, Eugene, OR]). The sections were then examined using a fluorescence microscope.

To quantify immunoreactivity, we counted the total number of ATF3 immunoreactive neurons (ATF3-IR neurons) and both ATF3 and GAP-43 immunoreactive neurons (ATF3/GAP-43 dual-IR neurons) in profile in every third section across each harvested DRG. Moreover, immunoreactive neurons were divided into two groups according to their cell diameter: small (<30 μm) and large (>30 μm) neurons, as determined by a graticule scale. All data was analysed by a blinded observer.

Statistical significance of differences between the ESW group and the control was determined by Tukey's test for equal sample variance with a confidence level greater than 95% ($P<0.05$).

Scattered ATF3-IR neurons were observed in DRG of the ESW group (Fig. 1A). In contrast, ATF3-IR neurons were rarely detected in DRG of the control group (Fig. 1B). Many aspects of ATF3-IR neurons seemed to also be immunoreactive for GAP-43 (Fig. 1C).

The average number of ATF3-IR neurons and ATF3/GAP-43 dual-IR neurons was significantly larger in the ESW group than in the control group at all time points (Fig. 2). The number of neither the ATF3-IR neurons nor the ATF3/GAP-43 dual-IR neurons showed a significant time dependence during the period studied (Fig. 2).

In total of all time points, 1969 immunoreactive neurons were observed in the ESW group (Table 1). The ratios of small neurons and large neurons to the total ATF3-IR neurons were 22.5% (444/1969) and 77.5% (1525/1969), respectively; 78.3% (1542/1969) of ATF3-IR neurons were also immunoreactive for GAP-43. Among the ATF3-IR neurons, 44.3% (197/444) of small neurons and 88.1% (1345/1525) of large neurons were also immunoreactive for GAP-43. The ratios of small and large ATF3/GAP-43 dual-IR neurons to the total ATF3/GAP-43 dual-IR neurons were 12.8% (197/1542) and 87.2% (1345/1542), respectively. The neurons immunoreactive for GAP-43 alone seemed to be in the majority, although we had not counted them precisely.

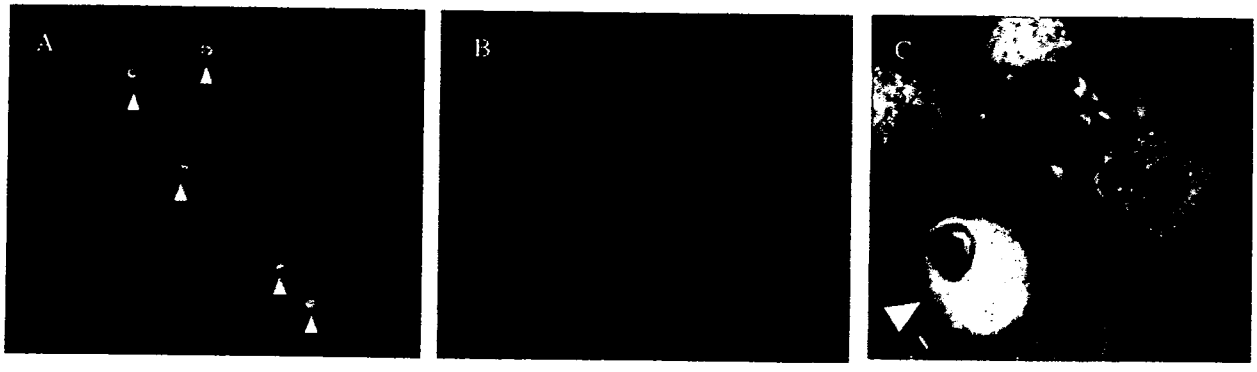

Fig. 1. Fluorescence microscopic images of dorsal root ganglion (DRG). A (×100): A section from L5 DRG in the ESW group 4 days after application of ESW. Several neurons with well-stained nuclei immunoreactive for ATF3 (arrowheads) are observed. B (×100): A section from L5 DRG in the control group. ATF3-IR neurons could not be detected in this section. C (×400): Merged images from L5 DRG in the ESWT group of 2 days after ESWT. An ATF3/GAP-43 dual-IR neuron with a well-stained nucleus and cytoplasm (arrowhead) is shown.

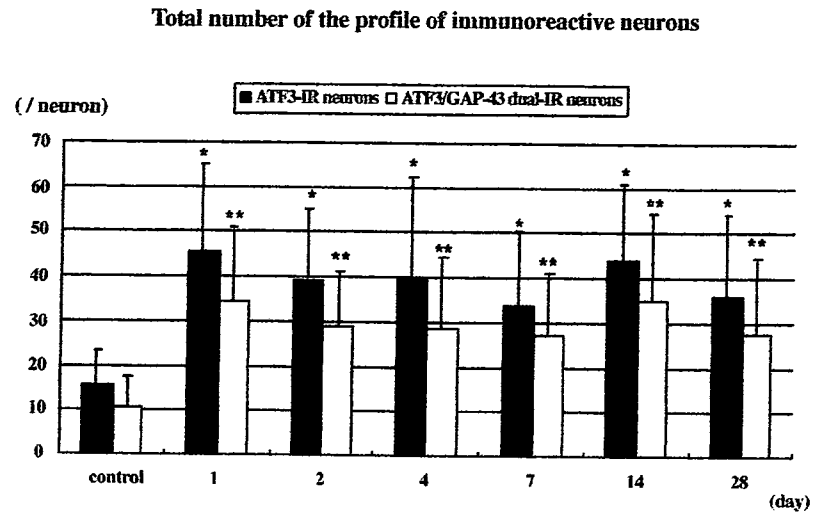

Fig. 2. Total profile of immunoreactive neurons. ATF3-IR neurons: neurons immunoreactive for ATF3. ATF3/GAP-43 dual-IR neurons: neurons immunoreactive for both ATF3 and GAP-43. This graph illustrates the total number of ATF3-IR neuron profiles (black column) and ATF3/GAP-43 dual-IR neuron profiles (white column). The symbols (*, **) indicate the significance of the difference of the data by Tukey's test compared to controls ($n=4$, $P<0.05$). All data were shown as mean values+S.D.

In this study, we showed that ESW to the rat footpad caused nerve injury as indicated by increased numbers of ATF3-IR neurons, and axonal regeneration by those neurons double labeled for ATF3 and GAP-43 immunoreactivity.

ATF3 is involved in the stress response (Hai et al., 1999). ATF3 is also known as a transcriptional repressor and is implicated in the cell death of some non-neuronal cells (Chen et al., 1994; Mashima et al., 2001; Nawa et al., 2002; Zhang et al., 2001). In the nervous system, ATF3 has been designated as a marker for nerve injury because of its specific expression in response to nerve injury (Tsujino et al., 2000; Obata et al., 2003). The rat model for nerve damage utilizing resection of the sciatic nerve has produced ATF3 immunoreactivity in a majority of DRG neurons (Tsujino et al., 2000; Obata et al., 2003), whereas our model showed fewer ATF3-IR neurons. Although the functional consequence of ATF3 in nerve injury has not been elucidated, this difference of ATF3 immunoreactivity may be related to a difference in the number of affected nerve fibers. The lithotripter we used generated focused shockwaves with an exposure area of approximately $5\times5\times26$ mm. The small number of nerve fibers within this area of narrow exposure might only be expected to produce weak ATF3 expression on the corresponding DRG, which is consistent with our observations.

Table 1
Size distribution of immunopositive neurons of the ESW group

	ATF3-IR neurons	
	ATF3/GAP-43 dual-IR neurons	Total
Small (<30 μm)	197	444
Large (>30 μm)	1345	1525
Total	1542	1969

This table shows the total number of immunopositive neurons of the ESW group. All data indicate combined number of all time points. Immunoreactive neurons were classified according to cell diameter measured by graticule scale as small (<30 μm) and large (>30 μm). All values were shown as the number of neurons in each category.
ATF3-IR neurons: neurons immunoreactive for ATF3.
ATF3/GAP-43 dual-IR neurons: neurons immunoreactive for both ATF3 and GAP-43.

In general, there is no simple correlation between epidermal innervation and sensory functions such as nociception (Lindenlaub and Sommer, 2002). Spinal and peripheral nerve injury often accounts for neuropathic or phantom pain (Chung et al., 1993; Devor et al., 1994; Ma and Bisby, 2000; McLachlan et al., 1993; O'Halloran and Perl, 1997; Verdu and Navarro, 1997). Previous clinical research focusing on ESW has shown significant pain relief and only few side effects, with a particular absence of problems such as neuropathic pain (Gerdesmeyer et al., 2003; Rompe et al., 1996, 2004). Thus, the increase of ATF3-IR DRG neuron number induced by ESW may be linked to the desensitization of the exposure area, not the cause of the neuropathic pain.

The significant increase in the number of ATF3-IR neurons after exposure was sustained for at least 28 days (Fig. 2). This observation, however, does not confirm a persistent desensitization of the exposed area. The presence of ATF3/GAP-43 dual-IR neurons, which account for 78.3% (1542/1969) of ATF3-IR neurons, may indicate the regeneration of injured nerve fibers (Table 1). GAP-43 is a 24 kDa neuronal-specific phosphoprotein, which is implicated in axogenesis and synaptogenesis during regeneration of the nervous system (Karns et al., 1987; Bomze et al., 2001). The expression of GAP-43 mRNA is induced early in the cell soma and proximal axon after axotomy (Hoffman, 1989; Verge et al., 1990; Tetzlaff et al., 1991). In the current study,

GAP-43 immunoreactivity was represented by exclusively well-stained cytoplasm, which had supported this finding. The regeneration phase of injured nerve fibers, indicated by the expression of ATF3/GAP-43 dual-IR neurons, began within a day of the ESW application. We found that most of the nerve fibers degenerated by ESW reinnervated the exposure area, penetrating the basal lamina of the epithelium within 14 days of the ESW application (Ohtori et al., 2001). The time difference in these findings suggests that actual elongation of damaged nerve fibers to the skin may require longer than GAP-43 expression in neuron after the ESW application. This rapid reinnervation of the exposed area could contribute to the amelioration of desensitization.

With regard to the size distribution of ATF3-IR neurons, 22.5% (444/1969) were classified as small neurons (Table 1). The sensory nerve fibers originating from small neurons are mainly of small diameter, suggesting their involvement in nociception, temperature perception and autonomic effects. Adrenergic sprouting induced after nerve lesions in nociceptive C-fibers (Sato and Perl, 1991) and DRG (McLachlan et al., 1993; Ramer et al., 1998) is thought to result from states of neuropathic pain. Thus, the injury of nerve fibers originating from small ATF3-IR neurons may be associated with the alleviation of pain.

However, 44.3% (197/444) of ATF3-IR small neurons also showed immunoreactivity for GAP-43 (Table 1), possibly indicating axonal regeneration of the injured small-diameter fibers. This proportion is much higher than the previously reported proportion of approximately 3% in normal DRG immunoreactive neurons in rats (Gonzalez-Hernandez and Rustioni, 1999). The up-regulation of ATF3/GAP-43 dual-IR small neurons most likely represented active axonal regeneration of the injured nerve fibers, which may indicate the recurrence of pain.

Moreover, 77.5% (1525/1969) of ATF3-IR neurons were classified as large neurons (Table 1). Most ATF3-IR DRG neurons had been observed in the rat sciatic nerve resection model are of medium to large diameter (Obata et al., 2003), indicating that large-diameter fibers such as Aα or Aβ fibers account for most of the injury, and small-diameter fibers such as Aδ or C-fibers were relatively uninjured. Although a difference in vulnerability between these fibers has not been established (Fröhling et al., 1998), large-diameter fibers are thought to be more sensitive to ESW than small-diameter fibers. These observations may help explain the analgesic effect of ESW, since large-diameter fibers play a crucial role in painful conditions such as allodynia (McLachlan et al., 1993).

This study has several potential limitations. We have counted the profile of immunoreactive neurons, but could not estimate the actual number of immunoreactive neurons (Coggeshall and Lekan, 1996). We examined DRG neurons immunohistochemically, but we did not directly evaluate any pain associated with the cellular effects observed. The analgesic effect of ESW may not be proven by physiological examination employing normal animal models. Study of the analgesic effects of ESW, especially physiological effects, should perhaps utilize pathological models of pain. The relevance of cellular ATF3 or GAP-43 levels with regard to the analgesic effect in clinical subjects has not been elucidated.

Nevertheless, this study shows that ESW induced peripheral nerve injury and regeneration of the nerve fibers originating from DRG neurons in rats, and that the nerve injury may contribute to the desensitization of the exposed area. The regeneration of injured nerve fibers may occur immediately after exposure and account for the reinnervation of the exposed area. These observations provide a partial explanation for the analgesic effects of ESW and may contribute to the elucidation of pain recurrence observed in clinical subjects.

References

Bomze, H.M., Bulsara, K.R., Iskandar, B.J., Caroni, P., Skene, J.H., 2001. Spinal axon regeneration evoked by replacing tow growth cone proteins in adult neurons. Nat. Neurosci. 4, 38–43.

Chen, B.P., Liang, G., Whelan, J., Hai, T., 1994. ATF3 and ATF3 delta Zip. Transcriptional repression versus activation by alternatively spliced isoforms. J. Biol. Chem. 269, 15819–15826.

Chung, K., Kim, H.J., Na, H.S., Park, M.J., Chung, J.M., 1993. Abnormalities of sympathetic innervation in the area of an injured peripheral nerve in a rat model of neuropathic pain. Neurosci. Lett. 162, 85–88.

Coggeshall, R.E., Lekan, H.A., 1996. Methods for determining numbers of cells and synapses: a case for more uniform standards of review. J. Comp. Neurol. 364, 6–15.

Coggins, P.J., Zwiers, H., 1991. B-50 (GAP-43): biochemistry and functional neurochemistry of a neuron-specific phosphoprotein. J. Neurochem. 56, 1095–1106.

Devor, M., Janig, W., Michaelis, M., 1994. Modulation of activity in dorsal root ganglion neurons by sympathetic activation in nerve-injured rats. J. Neurophysiol. 71, 38–47.

Fröhling, M.A., Schlote, W., Wolburg-Buchholz, K., 1998. Nonselective nerve fibre damage in peripheral nerves after experimental thermocoagulation. Acta Neurochir. 140, 1297–1302.

Gerdesmeyer, L., Wagenpfeil, S., Haake, M., Maier, M., Loew, M., Wortler, K., Lampe, R., Seil, R., Handle, G., Gassel, S., Rompe, J.D., 2003. Extracorporeal shock wave therapy for the treatment of chronic calcifying tendonitis of the rotator cuff: a randomized controlled trial. JAMA 290, 2573–2580.

Gonzalez-Hernandez, T., Rustioni, A., 1999. Nitric oxide synthase and growth-associated protein are coexpressed in primary sensory neurons after peripheral injury. J. Comp. Neurol. 404, 64–74.

Haake, M., Thon, A., Bette, M., 2002. Unchanged c-Fos expression after extracorporeal shock wave therapy: an experimental investigation in rats. Arch. Orthop. Trauma Surg. 122, 518–521.

Hai, T., Wolfgang, C.D., Marsee, D.K., Allen, A.E., Sivaprasad, U., 1999. ATF3 and stress responses. Gene Expression 7, 321–335.

Hoffman, P.N., 1989. Expression of GAP-43, a rapidly transported growth-associated protein, and class 2 beta tubulin, a slowly transported cytoskeletal protein, are coordinated in regenerating neurons. J. Neurosci. 9, 893–897.

Jacobson, R.D., Virag, I., Skene, J.H., 1986. A protein associated with axon growth, GAP-43, is widely distributed and developmentally regulated in rat CNS. J. Neurosci. 6, 1843–1855.

Karns, L.R., Ng, S.C., Freeman, J.A., Fishman, M.C., 1987. Cloning of complementary DNA for GAP-43, a neuronal growth-related protein. Science 236, 597–600.

Lindenlaub, T., Sommer, C., 2002. Epidermal innervation density after partial sciatic nerve lesion and pain-related behavior in the rat. Acta Neuropathol. 104, 137–143.

Ma, W., Bisby, M.A., 2000. Calcitonin gene-related peptide, substance P and protein gene product 9.5 immunoreactive axonal fibers in the rat footpad skin following partial sciatic nerve injuries. J. Neurocytol. 29, 249–262.

Maier, M., Averbeck, B., Milz, S., Refior, H.J., Schmitz, C., 2003. Substance P and prostaglandin E2 release after shock wave application to the rabbit femur. Clin. Orthop. Relat. Res. 406, 237–245.

Mashima, T., Udagawa, S., Tsuruo, T., 2001. Involvement of transcriptional repressor ATF3 in acceleration of caspase protease activation during DNA damaging agent-induced apoptosis. J. Cell. Physiol. 188, 352–358.

McLachlan, E.M., Janig, W., Devor, M., Michaelis, M., 1993. Peripheral nerve injury triggers noradrenergic sprouting within dorsal root ganglia. Nature 363, 543–546.

Nawa, T., Nawa, M.T., Adachi, M.T., Uchimura, I., Shimokawa, R., Fujisawa, K., Tanaka, A., Numano, F., Kitajima, S., 2002. Expression of transcriptional repressor ATF3/LRF1 in human atherosclerosis: colocalization and possible involvement in cell death of vascular endothelial cells. Atherosclerosis 161, 281–291.

Obata, K., Yamanaka, H., Fukuoka, T., Yi, D., Tokunaga, A., Hashimoto, N., Yoshinaga, H., Noguchi, K., 2003. Contribution of injured and uninjured dorsal root ganglion neurons to pain behavior and the changes in gene expression following chronic constriction model of the sciatic nerve in rats. Pain 101, 65–77.

O'Halloran, K.D., Perl, E.R., 1997. Effects of partial nerve injury on the responses of C-fiber polymodal nociceptors to adrenergic agonists. Brain Res. 759, 233–240.

Ohtori, S., Inoue, G., Mannoji, C., Saisu, T., Takahashi, K., Mitsuhashi, S., Wada, Y., Takahashi, K., Yamagata, M., Moriya, H., 2001. Shock wave application to rat skin induces degeneration and reinnervation of sensory nerve fibers. Neurosci. Lett. 315, 57–60.

Ramer, M.S., Murphy, P.G., Richardson, P.M., Bisby, M.A., 1998. Spinal nerve lesion-induced mechanoallodynia and adrenergic sprouting in sensory ganglia are attenuated in interleukin-6 knockout mice. Pain 78, 115–121.

Rompe, J.D., Hopf, C., Küllmer, K., Heine, J., Bürger, R., 1996. Analgesic effect of extracorporeal shock-wave therapy on chronic tennis elbow. J. Bone Jt. Surg. 78-B, 233–237.

Rompe, J.D., Decking, J., Schöellner, C., Theis, C., 2004. Repetitive low-energy shock wave treatment for chronic lateral epicondylitis in tennis players. Am. J. Sports Med. 32, 734–743.

Sato, J., Perl, E.R., 1991. Adrenergic excitation of cutaneous pain receptors induced by peripheral nerve injury. Science 251, 1608–1610.

Skene, J.H., Willard, M., 1981. Axonally transported proteins associated with axon growth in rabbit central and peripheral nervous system. J. Cell Biol. 89, 96–103.

Takahashi, Y., Nakajima, Y., Sakamoto, T., 1994. Dermatome mapping in the rat hindlimb by electrical stimulation of the spinal nerves. Neurosci. Lett. 168, 85–88.

Takahashi, N., Wada, Y., Ohtori, S., Saisu, T., Moriya, H., 2003. Application of shock wave to rat skin decreases calcitonin gene-related peptide immunoreactivity in dorsal root ganglion neurons. Auton. Neurosci. 107, 91–94.

Tetzlaff, W., Alexander, S.W., Miller, F.D., Bisby, M.A., 1991. Response of facial and rubrospinal neurons to axotomy: changes in mRNA expression for cytoskeletal proteins and GAP-43. J. Neurosci. 11, 2528–2544.

Tsujino, H., Kondo, E., Fukuoka, T., Dai, Y., Tokunaga, A., Miki, K., Yonenobu, K., Ochi, T., Noguchi, K., 2000. Activating transcription factor 3 (ATF3) induction by axotomy in sensory and motoneurons: a novel neuronal marker of nerve injury. Mol. Cell. Neurosci. 15, 170–182.

Verdu, E., Navarro, X., 1997. Comparison of immunohistochemical and functional reinnervation of skin and muscle after peripheral nerve injury. Exp. Neurol. 146, 187–198.

Verge, V.M., Tetzlaff, W., Richardson, P.M., Bisby, M.A., 1990. Correlation between GAP43 and nerve growth factor receptors in rat sensory neurons. J. Neurosci. 10, 926–934.

Zhang, C., Kawauchi, J., Adachi, M.T., Hashimoto, Y., Oshiro, S., Aso, T., Kitajima, S., 2001. Activation of JNK and transcriptional repressor ATF3/LRF1 through the IRE1/TRAF2 pathway is implicated in human vascular endothelial cell death by homocysteine. Biochem. Biophys. Res. Commun. 289, 718–724.

Available online at www.sciencedirect.com
SCIENCE DIRECT
Biomaterials 27 (2006) 3897–3903
Biomaterials
www.elsevier.com/locate/biomaterials

Mechanical and histological evaluation of a PMMA-based bone cement modified with γ-methacryloxypropyltrimethoxysilane and calcium acetate

Tadashi Tsukeoka[a], Masahiko Suzuki[a,*], Chikara Ohtsuki[b], Atsushi Sugino[b,c], Yoshikazu Tsuneizumi[a], Jin Miyagi[a], Kouichi Kuramoto[c], Hideshige Moriya[a]

[a]*Department of Orthopaedic Surgery, Graduate School of Medicine, Chiba University, 1-8-1 Inohana, Chuo-ku, Chiba 260-8677, Japan*
[b]*Graduate School of Materials Science, Nara Institute of Science and Technology, 8916-5 Takayama-cho, Ikoma-shi, Nara 630-0192, Japan*
[c]*Nakashima Medical Division, Nakashima Propeller Co. Ltd., 688-1 Jodo-Kitagata, Okayama 700-8691, Japan*

Received 20 November 2005; accepted 1 March 2006
Available online 24 March 2006

Abstract

Polymethylmethacrylate (PMMA) bone cement is widely used for prosthetic fixation in orthopaedic surgery; however, the interface between bone and cement is a weak zone. We developed a bioactive PMMA cement through modification with γ-methacryloxypropyltrimethoxysilane (MPS) and calcium acetate. The purpose of this study was to compare the handling, mechanical and histological properties of the modified bone cement with those of the conventional cement. The modified specimens exhibited higher bonding strength between bone and implant. Histological observation and micro-focus X-ray computed tomogram (micro-CT) images showed that the modified cement exhibited osteoconduction, which the conventional PMMA bone cement lacked. The modification was found to be effective in enabling osteoconduction with PMMA bone cement, thus providing stable fixation for a long period after implantation.

Keywords: Bioactivity; Bone cement; Mechanical property; In vitro test; In vivo test

1. Introduction

Polymethylmethacrylate (PMMA) bone cement has been widely used for prosthetic fixation in orthopaedic surgery. Among the zones that include prosthesis–bone cement–bone, the interface between bone and PMMA bone cement is known as one of the weak-link zones, because conventional PMMA bone cement is unable to bond to living bone [1]. One may expect that providing PMMA bone cement with bone-bonding ability, the so-called bioactivity, would solve the problem of fixation between living bone and PMMA bone cement.

Previously, powders of bioactive ceramics such as sintered hydroxyapatite and glass–ceramic A-W were added to PMMA bone cement [2,3] to fabricate bioactive bone cement. More than 60 wt% of bioactive ceramic powder should be included in PMMA powders to satisfy the osteoconductive properties after setting. Inadequate amounts of ceramic powder in the cement might leave less area of the bioactive fillers to react with the surrounding body fluid, on exposure to the body environment. Moreover, addition of excess amounts of ceramic power to the PMMA cement might adversely affect the mechanical and handling properties [4]. Modification of the methylmethacrylate (MMA) liquid is one of the possible methods to reduce the fraction of additives to the bioactive ceramic fillers, since the surface of the set cement should react with the surrounding body fluid. Previous studies on bone-bonding mechanisms of bioactive ceramics revealed that the essential requirement for an artificial material to bond to bone is the formation of an apatite layer on its surface after implantation in bony defects [5,6]. The apatite formation is triggered by the release of calcium ions (Ca^{2+}) from the surface of the bioactive materials, and by

*Corresponding author. Tel.: +81 43 222 7171; fax: +81 43 226 2116.
E-mail addresses: mdddd940@ybb.ne.jp (T. Tsukeoka), masahiko@med.m.chiba-u.ac.jp (M. Suzuki).

0142-9612/$ - see front matter © 2006 Elsevier Ltd. All rights reserved.
doi:10.1016/j.biomaterials.2006.03.002

the inductive effects of silanol (Si–OH) group on heterogeneous nucleation of the apatite layer under body environment [7]. Based on these mechanisms, we have proposed the development of a bioactive PMMA cement, modified with alkoxysilane compounds, which provides Si–OH groups, as well as calcium salts, which release Ca^{2+}. In our previous evaluation of several PMMA bone cements modified with alkoxysilane and calcium salts, the modification with 20 mass% of γ-methacryloxypropyltrimethoxysilane (MPS) and calcium acetate resulted in bioactive PMMA bone cement [8,9]. This modified PMMA was intended for prosthetic fixation. It should be noted that the quantity of additives in our modified cement was much lower than that in the previously reported method, i.e., 70 mass%. With this lower content of additives, our modified cement may exhibit better handling characteristics and mechanical properties. Few studies have reported the use of MPS in vivo, and hence toxicity of MPS in living tissue remains uncertain. In this study, the modified PMMA cement with MPS and calcium acetate was further evaluated to determine its handling characteristics, mechanical properties and behavior in a simulated body fluid (SBF). The possible problems with the application of the modified cement are discussed by comparing with the characters of commercially available conventional PMMA bone cement.

2. Materials and methods

2.1. Preparation of the modified PMMA bone cement

Modified PMMA bone cement was prepared according to a previous report [10]. The raw materials used for the preparation and the composition of modified PMMA bone cement are listed in Table 1. Calcium acetate monohydrate ($Ca(CH_3COO)_2 \cdot H_2O$) was pulverized to a size of less than 44 μm and calcined at 220 °C for 2 h in order to remove the water in the compounds. The PMMA powder that had an approximate molecular weight of 100,000 and average particle size of 14 μm was purchased from Sekisui Plastics Co. Ltd. The PMMA powder was mixed with heat-treated calcium acetate, as well as barium sulfate ($BaSO_4$) as radio-opaque filler and benzoyl peroxide (BPO) as polymerization initiator without further purification. The liquid components were prepared by mixing the chemical reagents, namely MMA, γ-MPS and *N,N*-dimethyl-*p*-toluidine (NDT) as polymerization accelerator. The paste was prepared by mixing the powder with the liquid at a powder-to-liquid (P/L) mass ratio of 2:1 under ambient conditions at room temperature. Zimmer® dough-type radio-opaque cement (Zimmer, Warsaw, IN, USA) was used as a reference of the commercialized conventional PMMA bone cement.

2.2. Measurement of the setting time and temperature during polymerization

Setting behavior of the mixed pastes was evaluated according to ISO5833 [11]. The paste, which was a mixture of the powder and liquid, was packed into a cylindrical mold (60 mm in diameter, 6 mm in height). The temperature measurement probe (CM-16635, HFT-40, Anritsu Meter Co. Ltd., Tokyo, Japan) was then installed into the center of the mold to measure the curing temperature every 20 s, until the temperature begins to fall. The maximum temperature, T_{max}, during polymerization was determined to plot the recorded temperature against time. The setting time was calculated using the following:

$$T = (T_{max} + T_{amb})/2, \quad (1)$$

where T was the setting temperature and T_{amb} was the recorded ambient temperature. The setting time was determined from the beginning of the mixing until the T value reaches. These experiments were carried out three times and the average and standard deviation calculated.

2.3. Compressive strength

For the compressive strength measurement, the cements were molded to the cylindrical specimens 6 mm in diameter and 12 mm in length. After curing, the cement was kept for 24 h in the air at room temperature. Moreover, molded specimens were exposed to SBF at 36.5 °C at a solution/surface area ratio = 0.1 ml/mm^2 before it was completely cured, and kept for 7 days. SBF proposed by Kokubo and his colleagues [12] was used in this study. Ion concentrations of SBF are Na^+ 142.0, K^+ 5.0, Mg^{2+} 1.5, Ca^{2+} 2.5, Cl^- 147.8, HCO_3^- 4.2, HPO_4^{2-} 1.0 and SO_4^{2-} 0.5 mM (= mol/m^3). The compressive load was applied at cross-head speed of 20 mm/min using the material testing machine (EHF-F01, Shimadzu Co., Kyoto, Japan) until fracture occurred. The compressive strength was calculated from compressive load and geometric area of the specimens. The average compressive strength and standard deviation were calculated.

2.4. Behavior of the specimen in SBF

Surface morphological changes and apatite formation on the cements after exposure to SBF were observed for the cements molded into rectangular shapes of 10 × 15 × 1 mm. Before the molded cements were completely cured, the specimens were immersed in 35 ml of SBF at 36.5 °C. After 1, 3 and 7 days, the specimens were removed from the solution, and gently washed with distilled water. Surface changes of the specimens were characterized by thin-film X-ray diffraction (TF-XRD, RINT2500, Rigaku Co., Tokyo, Japan), field emission scanning electron microscopy

Table 1
Composition of the examined cement

Components	Mass ratio	Note
Powder		
PMMA	0.680	Sekisui Plastics Co. Ltd., Tokyo, Japan
Calcium acetate ($Ca(CH_3COO)_2 \cdot H_2O$)	0.194	Wako Pure Chemicals Industries Ltd., Osaka, Japan
Benzoyl peroxide (BPO)	0.029	Wako Pure Chemical Industries Ltd., Osaka, Japan
Barium sulfate ($BaSO_4$)	0.097	Sakai Chemical Industry Co. Ltd., Osaka, Japan
Liquid		
Methylmethacrylate (MMA) monomer	0.397	Wako Pure Chemical Industries Ltd., Osaka, Japan
N,N-dimethyle-*p*-toluidine (NDT)	0.004	Kanto Chemical Co. Inc., Tokyo, Japan
γ-Methacryloxypropyl-trimethoxysilane (MPS)	0.099	Chisso Industry Co. Ltd., Tokyo, Japan